A monocyte/dendritic cell molecular signature of SARS-CoV-2-related multisystem inflammatory syndrome in children with severe myocarditis

Camille de Cevins, Marine Luka, Nikaïa Smith, Sonia Meynier, Aude Magérus, Francesco Carbone, Víctor García-Paredes, Laura Barnabei, Maxime Batignes, Alexandre Boullé, et al.

Version of Record: https://www.sciencedirect.com/science/article/pii/S2666634021002877
Manuscript_1054a616150ebaeb3bfe4ade78944251

A monocyte/dendritic cell molecular signature of SARS-CoV-2 related multisystem inflammatory syndrome in children (MIS-C) with severe myocarditis

Camille de Cevins[1, 2], Marine Luka[1, 3, #], Nikaïa Smith[4, #], Sonia Meynier[5, #], Aude Magérus[5, #], Francesco Carbone[1, 3, §], Víctor García-Paredes[1, 3, §], Laura Barnabei[5, §], Maxime Batignes[1], Alexandre Boullé[1], Marie-Claude Stolzenberg[5], Brieuc P. Pérot[1], Bruno Charbit[6], Tinhinane Fali[1], Vithura Pirabarakan[5], Boris Sorin[5], Quentin Riller[5], Ghaith Abdessalem[1], Maxime Beretta[7,8], Ludivine Grzelak[9], Pedro Goncalves[10,11], James P. Di Santo[10,11], Hugo Mouquet[7,8], Olivier Schwartz[9], Mohammed Zarhrate[12], Mélanie Parisot[12], Christine Bole-Feysot[12], Cécile Masson[13], Nicolas Cagnard[13], Aurélien Corneau[14] , Camille Bruneau[5], Shen-Ying Zhang[15,16], Jean-Laurent Casanova[15,16,17], Brigitte Bader Meunier[17], Julien Haroche[18], Isabelle Melki[17,19], Mathie Lorrot[20], Mehdi Oualha[21], Florence Moulin[21] Damien Bonnet[22], Zahra Belhadjer[22], Marianne Leruez[23], Slimane Allali[24], Christèle Gras Leguen[25], Loïc de Pontual[26], Pediatric-Biocovid Study Group, Alain Fischer[17, 27, 28], Darragh Duffy[4, 6, *], Frédéric Rieux-Laucat[5, *, ^], Julie Toubiana[24, 29, *], Mickaël M. Ménager[1, 3, *, ^, ∞]

Affiliations

1. Université de Paris, Imagine Institute, Laboratory of Inflammatory Responses and Transcriptomic Networks in Diseases, Atip-Avenir Team, INSERM UMR 1163, F-75015 Paris, France.
2. Molecular Biology and Genomics, Translational Sciences, Sanofi R&D, Chilly-Mazarin, France.
3. Labtech Single-Cell@Imagine, Imagine Institute, INSERM UMR 1163, F-75015 Paris, France.
4. Translational Immunology Lab, Department of Immunology, Institut Pasteur, F-75015 Paris, France.
5. Université de Paris, Imagine Institute Laboratory of Immunogenetics of Pediatric Autoimmune Diseases, INSERM UMR 1163, F-75015 Paris, France.
6. Cytometry and Biomarkers UTechS, CRT, Institut Pasteur, F-75015, Paris
7. Humoral Immunology Laboratory, Department of Immunology, Institut Pasteur, F-75015, Paris
8. Inserm U1222, Institut Pasteur, F-75015, Paris
9. Virus and Immunity Unit, Department of Virology, Institut Pasteur, F-75015, Paris
10. Inserm U1223, Institut Pasteur, F-75015, Paris
11. Innate Immunity Unit, Department of Immunology, Institut Pasteur, F-75015, Paris
12. Genomics Core Facility, Institut Imagine-Structure Fédérative de Recherche Necker, INSERM U1163 et INSERM US24/CNRS UMS3633, Paris Descartes Sorbonne Paris Cite University, Paris, France
13. Bioinformatics Platform, Structure Fédérative de Recherche Necker, INSERM UMR1163, Université de Paris, Imagine Institute, Paris, France.
14. Sorbonne Université, UMS037, PASS, Plateforme de cytométrie de la Pitié-Salpêtrière CyPS, F-75013 Paris, France
15. Université de Paris, Imagine Institute, Laboratory of Human Genetics of Infectious Diseases, Necker Branch, INSERM, F-75015 Paris, France.
16. St. Giles Laboratory of Human Genetics of Infectious Diseases, Rockefeller Branch, The Rockefeller University, New York, NY, USA
17. Department of Paediatric Immuno-Haematology and Rheumatology, Reference center for Rheumatic, AutoImmune and Systemic diseases in children (RAISE), Hôpital Necker-Enfants Malades, Assistance Publique - Hôpitaux de Paris (AP-HP) F-75015 Paris, France
18. Department of Immunology and Infectious disease (CIMI-Paris), Pitié-Salpêtrière University Hospital, Sorbonne université, AP-HP, F-75013 Paris, France
19. Department of Pediatrics, Robert-Debré University Hospital, AP-HP, Université de Paris, Paris, France
20. Department of Pediatrics, Armand-Trousseau University Hospital, AP-HP, F-75012 Paris, France

21. Pediatric Intensive Care Unit, Necker-Enfants Malades University Hospital, AP-HP, Université de Paris, F-75015 Paris, France
22. M3C-Necker Enfants Malades, AP-HP, Paris, France
23. Virology laboratory, Necker-Enfants Malades University Hospital, AP-HP, Université de Paris, F-75015 Paris, France
24. Department of General Paediatrics and Paediatric Infectious Diseases, Necker-Enfants Malades University Hospital, Assistance Publique - Hôpitaux de Paris (AP-HP), Université de Paris, F-75015 Paris, France
25. Pediatric Department, Nantes University Hospital, Nantes, FR-44000, France
26. Department of Pediatrics, Jean Verdier Hospital, Assistance Publique-Hôpitaux de Paris, Paris 13 University, Bondy, France
27. Université de Paris, Imagine Institute, INSERM UMR 1163, F-75015 Paris, France.
28. Collège de France, Paris, France.
29. Institut Pasteur, Biodiversity and Epidemiology of Bacterial Pathogens, Paris, France.

[#] Contributed equally
[§] Contributed equally
* Contributed equally
[^] **Corresponding authors**
[∞] **Lead Contact**

Correspondence:
MM : mickael.menager@institutimagine.org
FRL : frederic.rieux-laucat@inserm.fr

Abstract

Background

SARS-CoV-2 infection in children is generally milder than in adults, yet a proportion of cases result in hyperinflammatory conditions often including myocarditis.

Methods

To better understand these cases, we applied a multi-parametric approach to the study of blood cells of 56 children hospitalized with suspicion of SARS-CoV-2 infection. Plasma cytokine and chemokine levels and blood cellular composition were measured, alongside gene expression both at the bulk and single cell levels.

Findings

The most severe forms of multisystem inflammatory syndrome in children related to SARS-CoV-2 (MIS-C), that resulted in myocarditis, were characterized by elevated levels of pro-angiogenesis cytokines and several chemokines. Single-cell transcriptomic analyses identified a unique monocyte/dendritic cell gene signature that correlated with the occurrence

of severe myocarditis, characterized by sustained NF-□B activity, TNF-□ signaling, associated with decreased gene expression of NF-κB inhibitors. We also found a weak response to type-I and type-II interferons, hyperinflammation and response to oxidative stress related to increased HIF-1□ and VEGF signaling.

Conclusions

These results provide potential for a better understanding of disease pathophysiology.

Funding

Agence National de la Recherche (Institut Hospitalo-Universitaire Imagine, grant ANR-10-IAHU-01, Recherche Hospitalo-Universitaire, grant ANR-18-RHUS-0010, Laboratoire d'Excellence ''Milieu Intérieur", grant ANR-10-LABX-69-01, ANR-flash Covid19 "AIROCovid" and "CoVarImm"), Institut National de la Santé et de la Recherche Médicale (INSERM) and the "URGENCE COVID-19" fundraising campaign of Institut Pasteur

Introduction

In adults, critical forms of COVID-19 are typically characterized by severe pneumonia and acute respiratory distress syndrome[1]. In children, symptomatic COVID-19 occurs much less frequently and is milder than in adults for reasons that remain poorly understood[2–6]. However, in regions with high incidence of SARS-CoV-2 infection, some children have presented a postacute hyperinflammatory illness[7]. In these cases, diagnostic evidence of recent SARS-CoV-2 infection has been consistently reported[8–11]. This condition was named multisystem inflammatory syndrome in children (MIS-C) or alternatively PIMS-TS (Pediatric Inflammatory Multisystem Syndrome Temporally Associated with SARS-CoV-2)[12]. MIS-C cases can present with symptoms similar to Kawasaki Disease (KD), an hyperinflammatory illness characterized by clinical features such as strawberry-like tongue and red and dry lips, bulbar conjunctival injection, diffuse rash, swollen extremities and cervical

lymphadenopathy[13]. KD complications can develop as myocarditis or shock syndrome in a minority of cases[14]. KD is thought to be triggered by viral or bacterial pathogens but the precise pathophysiological mechanisms remain elusive[15]. Compared to classic KD, MIS-C occurs in patients who are older, have more often gastrointestinal symptoms, myocarditis and shock syndrome, and exhibit higher levels of inflammatory markers[7,8,10,11].

Inflammatory features of MIS-C are in part overlapping with those of both KD and acute SARS-CoV-2 infection in children, as well as severe COVID-19 in adults[7,16–18]. Very high levels of C-reactive protein (CRP), Procalcitonin (PCT) and IL-6, might reflect a strong immunological response to a pathogenic SARS-CoV-2 superantigen[19].

To further decipher SARS-CoV-2-related conditions in children, we have performed a detailed multi-parametric study combining sensitive cytokine measurements, deep immune cell phenotyping and transcriptomic analyses at the single-cell level on peripheral blood mononuclear cells (PBMCs). We first compared data from children with SARS-CoV-2 acute infection and postacute hyperinflammation, and then analyzed pathways and molecular signatures characteristic of the most severe form of MIS-C with severe myocarditis.

Results

Clinical description of the cohort

The study cohort consisted of 56 children hospitalized during the first peak of the SARS-CoV-2 pandemic (from the 6th of April to the 30th of May 2020), and 34 healthy controls (N=26 pediatric and N=8 adults recruited before the COVID-19 pandemic) (**Figure 1, Table S1**). Among the 13 children with acute respiratory infection suspected of SARS-CoV-2 (**Table S1, Figure S1**), 9 had a confirmed SARS-CoV-2 infection (RT-PCR on

nasopharyngeal aspiration or swab) (*Acute-inf (CoV2$^+$)* group). Six out of these 9 cases had pneumonia, and one had an uncomplicated febrile seizure. Antibiotic therapy was given to 3/9 patients. Only one patient with a history of recent bone marrow transplantation for sickle cell disease required intensive care support and received tocilizumab. The 4 other patients (*Acute-inf (CoV2$^-$)* group) had pneumonia associated with a positive RT-PCR test for either *Mycoplasma pneumoniae* or rhinovirus/enterovirus, and negative RT-PCR for SARS-CoV-2.

Forty-three children displayed features of postacute hyperinflammatory illness (**Figure S1, Table S1**). SARS-CoV-2 infection status of all samples was confirmed by specific antibody determination (IgG and IgA) in the plasma, using ELISA and flow cytometry-based technics (**Figure S2A**). Most (n=30) had confirmed SARS-CoV-2 infection (with 14 also positive for concomitant nasopharyngeal RT-PCR testing) and were therefore considered as cases of MIS-C (*MIS-C (CoV2$^+$)* group); all 30 cases of MIS-C presented clinical features of KD, 14 of them fulfilled clinical criteria for a complete form of KD according to the American Heart Association[13]. Of note, 21/30 cases had severe myocarditis (i.e. with elevated high-sensitivity cardiac troponin I and/or regional wall motion abnormalities on echocardiography, and clinical signs of circulatory failure requiring intensive care support; *MIS-C_MYO (CoV2$^+$)*). Thirteen tested negative for SARS-CoV-2 and fulfilled clinical criteria for complete (n=6) or incomplete (n=7) Kawasaki disease (KD), and were therefore considered to have KD-like illness (*KD (CoV2$^-$)* group) (**Figure S1, Table S1**). Clinical and biological characteristics, at time of disease activity and before treatment, or within 24 hours of treatment onset, are presented in **Table S1.** Most children (41/43) with postacute hyperinflammation received intravenous immunoglobulin (IVIG) injections, many of them shortly after admission and therefore before inclusion and sampling (N=7 out of 9 in *MIS-C (CoV2$^+$);* N=20 out of 21 in *MIS-C_MYO (CoV2$^+$)*; N=11 out of 13 in *KD (CoV2$^-$)*. The adjunction of corticosteroids was

decided by the clinician in 16 out of the 43 cases, mostly because of either initial severity, high risk of IVIG unresponsiveness[20], or IVIG unresponsiveness. They were administered before sampling for some of them (N=1 in *MIS-C ($CoV2^+$);* N=7 in *MIS-C_MYO ($CoV2^+$)*; N=4 in *KD ($CoV2^-$)*). All cases responded favorably to IVIG alone or in combination with glucocorticosteroids. MIS-C cases had low lymphocyte counts and those with severe myocarditis had abnormally increased neutrophil counts as compared to other groups, along with high levels of C-reactive protein (CRP), procalcitonin (PCT), serum alanine transaminases (ALT) and ferritin (**Table S1**). Multi-parametric analyses were performed at a median fever persistence of 9-10 days (**Figures 1A, B**) and focused on children with acute infection and postacute hyperinflammation related to confirmed SARS-CoV-2 infection.

Elevated inflammatory cytokine levels in pediatric acute infection and postacute hyperinflammatory conditions

We investigated plasma cytokine and chemokine levels in all patients by multiplexed or ultrasensitive ELISA assays. Hierarchical clustering analysis and stratification by patient groups revealed overall elevated levels of immune and inflammatory markers, with 40/46 measured proteins significantly elevated (q<0.05) compared to healthy controls (**Figure 2A and S2B**; global heat map). Thirteen cytokines were found to be elevated in all groups of patients compared to healthy controls **(Figure S2C).** High IL-8 and CXCL1 (**Figure 2C)** were more specific to children with acute infection. Cytokine levels did not significantly differ in children with acute infection with or without evidence of SARS-CoV-2 infection (**Figures S2B**). IFN-α2, IFN-γ, IL-17A, TNF-α, and IL-10 were higher in children with postacute hyperinflammation (*MIS-C ($CoV2^+$)*, *MIS-C_MYO ($CoV2^+$)*, than in pediatric healthy donors (CTL) and patients with acute infections (*Acute-inf ($CoV2^+$)* and were also found elevated in the *KD ($CoV2^-$)* group (**Figures 2A, B, S2B**).

Altogether, high inflammatory cytokine levels were detected in both acute infection and postacute inflammatory cases. Even though most patients with postacute hyperinflammation received IVIG and/or corticosteroids before sampling, the strongest inflammatory profile is observed in MIS-C. As both IVIG and corticosteroids are known immune modulators, differences between acute infection and postacute hyperinflammation are unlikely due to the treatments[21,22]. Nevertheless, IVIG treatment could account for the increase of anti-inflammatory mediators such as IL-10, IL-1RA and TGF-β1, as previously reported[23–26]. We could not assess the specific effects of IVIG treatment as almost all postacute cases were treated by IVIG before sampling, however the inflammatory profile was much reduced in intensity in MIS-C cases under combined glucocorticosteroid and IVIG treatment, as compared to IVIG alone (**Figure 2A**).

Low monocyte and dendritic cell frequencies in patients with postacute hyperinflammatory illness

To better decipher the blood immune cell composition of each group, PBMCs were analyzed by CyTOF mass spectrometry and by single-cell analyses at the transcriptomic level (SC-RNA-SEQ) (**Figure 1**). Regarding CyTOF and single-cell analyses, all MIS-C patients were treated with IVIG, and only one patient in the group with severe myocarditis also received glucocorticosteroids before sampling. Clustering analyses of the data obtained from CyTOF and SC-RNA-SEQ revealed consistent results, with most of the alterations observed in clusters composed of monocytes or dendritic cells (DCs) (**Figures 3A, B; S3 A-D**). The most drastic changes were a decrease in conventional DCs (cDCs) and plasmacytoid DCs (pDCs) in patients with a postacute hyperinflammatory illness ((*MIS-C_MYO (CoV2$^+$), MIS-C (CoV2$^+$)* and *KD (CoV2$^-$)*). As previously reported[18], we also observed a trend towards a decrease in monocyte clusters in children with postacute hyperinflammatory illness, that was

found independently of SARS-CoV-2 status (**Figures 3A, B; S3A-D**). Of note, it has been reported that in some cases, IVIG treatment could impair DC function and decrease monocytes and DC proportions[23,25,27–31]. In addition, some heterogeneity was observed in the proportions of non-classical monocytes in *Acute-Inf (CoV2$^+$)* cases and additional heterogeneity in the proportions of classical and intermediate monocytes in patients with severe myocarditis (*MIS-C_MYO (CoV2$^+$)* (**Figures 3A, B**), but there was no correlation with clinical data, including treatments, age (**Table S1**), nor cytokine/chemokine measurements (**Figures 2 and S2**). Additional modifications were detected in patients with acute SARS-CoV-2 infection (*Acute-inf (CoV2$^+$)* cases), consisting in a decrease of MAIT cells and an excess of naïve and central memory CD4$^+$ T cells (**Figures 3A, B, S3 C, D**). As the median age is very low in this group (0.2 years, **Table S1**) as compared to other groups, we cannot exclude an age effect.

Overexpression of inflammatory pathways, NF-κB signaling, and metabolic changes related to hypoxia in acute infection and postacute hyperinflammatory conditions

To gain further insight into the mechanisms behind acute infection and postacute hyperinflammation driven by SARS-CoV-2 in children, we assessed pathways modulated in each group by looking at the differentially expressed genes, obtained from the SC-RNA-SEQ dataset. In patients with acute infection (*Acute-inf (CoV2$^+$) and Acute-inf (CoV2$^-$)*), the numbers of differentially expressed genes were homogeneously distributed among monocytes/DCs, T and B cells (**Figures 4A and S4A).** Pathway enrichment analyses revealed a decrease in oxidative phosphorylation, coupled with an increase of HMGB1 signaling, HIF-1α signaling, and hypoxia signaling (**Figure 4B**). Production of nitric oxide was observed in both groups of acute infections, independently of SARS-CoV-2 infection, as compared to healthy controls (**Figure S4B**). These observations suggest a metabolic switch

potentially driven by hypoxic conditions. NF-κB signaling, VEGF signaling and inflammatory pathways (type-I and type-II IFNs, IL-1, IL-6, and IL-17 signaling pathways) were also found to be overrepresented in both groups of patients (**Figure S4B**).

Interestingly, alterations in the same pathways were also identified in all cases of children with SARS-CoV-2-related postacute illnesses (*All MIS-C (CoV2$^+$)*: *MIS-C_MYO (CoV2$^+$)* and *MIS-C (CoV2$^+$)*). However, in these cases, alterations were mostly restricted to monocytes and DCs (**Figures 4A, B**). Comparisons of genes differentially expressed between children with postacute hyperinflammatory illness with or without evidence of SARS-CoV-2 infection (*All MIS-C (CoV2$^+$)* versus *KD (CoV2$^-$)*), did not reveal significant differences except for type-I and type-II interferon signaling (**Figures S4C, D)**.

The NF-κB signaling pathway was identified to be activated in monocytes and DCs of all patients with acute infection and postacute hyperinflammatory illness, independently of SARS-CoV-2 infection (**Figure 4C**). While monocytes and DCs of patients with acute infection (*Acute-inf (CoV2$^+$)* highly expressed genes of the NF-κB complex (*REL*, *RELA*, *RELB*, *NFKB1*, *NFKB2*; **Figure 4D**), monocytes and DCs from all MIS-C patients (*MIS-C_MYO (CoV2$^+$)* and *MIS-C (CoV2$^+$)*) exhibited a strong decrease in the expression of NF-κB inhibitors, such as *NFKBIA, NFKBID, NFKBIE* and *NFKBIZ* (**Figures 4D**).

In conclusion, pathways dysregulated in acute infection or postacute hyperinflammatory illness, reflected an inflammatory status based on NF-κB signaling combined with changes in metabolism driven by a hypoxic environment. In acute respiratory disease, changes in gene expression reflected involvement of all PBMCs, whereas in postacute hyperinflammatory illnesses, monocytes/DCs were the most affected populations. These results further support the implication of monocyte/DC populations in MIS-C.

Exacerbated TNF-α and NF-κB signaling in MIS-C with severe myocarditis

To identify differences between patients with and without severe myocarditis, we compared cytokines/chemokines and gene expression profiles in patients treated with IVIG only before sampling. A slightly higher expression of TRAIL, IL-7, IL-2, IL-13, IFN-γ, IFN-α2, IL-17A and Granzyme B was found in MIS-C without myocarditis (*MIS-C ($CoV2^+$)* patients) (**Figures 5A and S5A**). In contrast, 17 cytokines and chemokines were higher in MIS-C with severe myocarditis (*MIS-C_MYO ($CoV2^+$)*) (**Figures 5A, B, S5B**). Of note, 9 of them are known to be associated with TNF-α and NF-κB signaling (**Figure 5B**). They are involved in propagation of inflammation (IL-6), angiogenesis and vascular homeostasis (VEGF and TGF cytokines) and activation, chemotaxis and migration of myeloid cells (CCL2, CX3CL1, CXCL10, CCL20, CCL3)[32,33]. An increased level of CCL19 (cell migration and chemotaxis) and IL-1 antagonist (IL-1RA) were also observed, as well as increased soluble PD-L1 (**Figure S5B**). Other noticeably elevated cytokines were CSF2 and CSF3 known to be involved in myeloid cell differentiation and migration (**Figure S5B**).

Regarding genes differentially expressed, most changes were observed in monocytes/DCs which led us to focus on these populations for the following analyses **(Figures S5C, D)**. A strong overexpression of genes belonging to TNF-α and NF-κB signaling was found in monocytes/DCs of MIS-C with severe myocarditis (*MIS-C_MYO ($CoV2^+$)*) **(Figure 5C)**. Strikingly, the decrease in the expression of NF-κB inhibitors observed in all MIS-C patients in **figure 4D**, appeared to be specific to the monocytes and DCs of MIS-C patients with severe myocarditis (*MIS-C_MYO ($CoV2^+$)*) (**Figure 5D**). Among the other pathways upregulated in *MIS-C_MYO ($CoV2^+$)*, we identified inflammatory responses, hypoxia, and response to oxidative stress (*HIF1A*, *HMOX1*, *HMBG1, etc.)* (**Figures S6A, B**). TGF-β signaling and VEGF signaling were also found enriched in monocytes and DCs of patients with myocarditis and to a lesser magnitude in B cells (**Figures S6A, B**).

To summarize, NF-κB activation, a decreased expression of NF-κB inhibitors, TNF-α signaling, together with a hypoxic response to oxidative stress and VEGF signaling, characterize the monocytes and DCs of children with MIS-C and severe myocarditis.

A lack of response to type-I and type-II IFN in MIS-C with severe myocarditis

Pathway enrichment performed both with IPA and EnrichR[34,35] highlighted the modulation of type-I and type-II interferon signaling pathways, with the upregulation of several interferon stimulated genes (ISGs) (*JAK2*, *STAT1*, *STAT2*, *IFITM1, IFITM2, IFI35, IFIT1, IFIT3, MX1, IRF1*) in monocytes/DCs, T and B cells of MIS-C patients without myocarditis only (**Figures 6A-D and S6A, C**). However, both groups of MIS-C patients showed elevated plasma IFN-α2 and IFN-γ proteins (**Figures 2A, B and 6A**). Gene expression downregulation in monocytes/DCs of MIS-C patients with severe myocarditis (included most of the MHC class II genes) suggests a decrease in antigen processing and presentation pathways (**Figure S6C**), alongside a downregulation of genes linked with oxidative phosphorylation, nitric oxide production and iNOS signaling which can be related to the establishment of hypoxic conditions and response to oxidative stress (**Figure S6A**). As all MIS-C patients analyzed in single-cell experiments have received IVIG prior to sampling, changes observed at the level of gene expression are unlikely to be biased by this treatment.

Identification of a molecular signature specific to MIS-C with severe myocarditis

To identify a potential clinical relevance of our study, we searched for a molecular signature that correlated with the appearance of severe myocarditis among the monocytes/DCs of children with SARS-CoV-2-related MIS-C. By using several SC-RNA-SEQ comparison strategies (**Figure 7A**), we identified 329 genes upregulated in monocytes/DCs of the MIS-C group with myocarditis (N=6) as compared to all other groups (**Figure 7A**). To validate this

molecular signature, RNA from PBMCs were sequenced from patients enrolled in our study but not analyzed by SC-RNA-SEQ. A scoring system was generated, based on normalized expression represented by a Z-score, coupled with hierarchical clustering, in order to identify genes that were overexpressed in children with myocarditis (*MIS-C_MYO (CoV2$^+$)* group) as compared to the other groups (**Figure S7A**). Within the 329 genes identified by SC-RNA-SEQ in monocytes and DCs of patients with severe myocarditis, expression of 116 genes were found upregulated in PBMCs from a group of 9 patients belonging to the *MIS-C_MYO (CoV2$^+$)* group with myocarditis and not analyzed by SC-RNA-SEQ (**Figures 7B**). From these genes, a signature score (SignatureSCORE) was determined for each sample processed by Bulk-RNA-SEQ (**Figure 7C**). We then further developed a RankingSCORE (**Figures S7 A, B**) to identify the top genes that contributed the most to the monocytes and DCs myocarditis signature. This led to the identification of a set of 25 genes that clearly segregate patients with severe myocarditis from other MIS-C (**Figure 7D)**. Consistently, most of these 25 genes belong to functional pathways that were previously identified (**Figures 5, S5, 6 and S6**), such as inflammation, oxidative stress, TNF-α and/or NF-κB signaling, and in some cases already known markers of myocarditis or MIS-C and/or COVID-19, such as genes coding for S100 proteins (**Figures S7C-E).** S100 proteins and calcium-binding cytosolic proteins are known to serve as danger signals to regulate cell migration, homeostasis and inflammation and were recently reported as new biomarkers for the most severe forms of COVID-19 in adults with acute severe respiratory syndrome[36].

Discussion

Multi-parametric analysis of PBMCs from children with acute respiratory infection and postacute hyperinflammation, collected during the COVID-19 pandemic, allowed to detect an inflammatory profile associated with a loss of circulating monocytes and dendritic cells (DCs), as well as an upregulation of genes and pathways involving NF-κB signaling, oxidative stress with establishment of hypoxic conditions and VEGF signaling. These pathways were upregulated in both acute and postacute groups of patients, independently of SARS-CoV-2 infection. However, significant features of MIS-C with severe myocarditis were detected specifically in monocytes and DCs including increased TNF-α and NF-κB signaling, decreased expression of NF-κB inhibitors, transcriptional responses corresponding to hypoxic conditions and low type-I and type-II IFN responses despite elevated cytokines detected in the plasma.

Acute cases were characterized by the detection of inflammatory markers in the plasma with a particularly strong elevation of IL-8 and CXCL1, two chemokines known to mediate neutrophil migration to the lung[37–39] and a modest elevation of IFN-α2 levels. These findings suggest that in some children, a suboptimal anti-viral type-I interferon response, alongside a hyperinflammatory response (IL-6 levels and exacerbation of the NF-κB pathway), could account for SARS-CoV-2 disease with pneumonia, as compared to the very usual benign or even asymptomatic clinical course of SARS-CoV-2 infection in children. This has been previously observed in severe Respiratory Syncytial Virus infections[40].

In the postacute patients treated by IVIG alone, elevated levels of plasma IFN-γ, IFN-α2, IL-10, IL-17, and, to a lesser extent, TNF-α, were found, as previously described in other cohorts[16–18,41,42]. These findings are typical of an ongoing anti-viral immune response, not directly related to SARS-CoV-2 infection. In addition, elevated chemokines such as CCL2, CCL3 and CCL4 may recruit monocytes and DCs to tissues, possibly accounting for their

reduced numbers observed in the blood of these patients. Additional mechanisms such as apoptosis or other cell death pathways may also be involved and we cannot exclude an effect of the IVIG treatment, as previously reported in some studies[23,27,28,30,31]. By comparison with children with acute infection, most of the patients with postacute hyperinflammation received IVIG treatment before sampling, with some combined with glucocorticosteroids. The immunosuppressive effects of glucocorticoids are identified at the cytokine/chemokine level. Nevertheless, IVIG treatment cannot account for the increase in inflammatory cytokines observed. However, IVIG treatment could explain the increase of anti-inflammatory mediators such as IL-10, IL-1RA and TGF-β1, observed in MIS-C[22–26,29].

Cellular phenotypes that distinguish MIS-C from classical KD have been previously reported[17,41,42]. Brodin and colleagues described several key differences such as elevated IL-17, IL-6 and CXCL10 that were only observed in KD, associated with decreased naïve $CD4^+$ T cells and increased central memory and effector memory $CD4^+$ T cells in MIS-C. In the present study, high levels of IL-17, IL-6 and CXCL10, were both found in MIS-C and in our KD ($CoV2^-$) groups. Differences observed in previous reports by Brodin and colleagues, may be due to the clinical homogeneity of our MIS-C group, as all had KD criteria. CDC and WHO case definitions show a much broader spectrum of disease, and Brodin *et al.*, like some clinical studies[8] may have included patients with multisystem involvement along with laboratory evidence of inflammation of MIS-C but without KD. Another explanation may be the time of blood sampling relative to admission to hospital and medical treatments. Third, we cannot exclude that our *KD ($CoV2^-$)* patients were different from 'classical' KD patients enrolled before the start of the COVID-19 pandemic. Altogether our data still support the hypothesis that MIS-C patients with KD features exhibit a molecular phenotype close to the

one seen in KD patients, suggesting overlapping pathogenesis mechanisms[18], although the impact of treatments received prior to sampling cannot be excluded.

Strikingly, we did find noticeable differences when comparing MIS-C with MIS-C cases associated with severe myocarditis and circulatory failure that required intensive care. The expression of several cytokines/chemokines was further increased in these cases, most of them related to the NF-κB−TNF-α signaling axis. Elevated VEGF and TGF-α and TGF-β are potential drivers of angiogenesis and vascular homeostasis, whereas elevated chemokines (CCL2, CCL3, CCL20, CX3CL1, CXCL10) could mediate increased cell migration towards inflamed tissues. Molecular analysis confirmed an upregulation of genes belonging to the TNF-α and NF-κB signaling pathways that were specifically found in monocytes and DCs of MIS-C patients with severe myocarditis. A lower expression of NF-κB complex inhibitors, including *TNFAIP3* (A20), *TNFAIP2, NFKBIA, NFKBIZ,* was detected, suggesting a possible mechanism for NF-κB sustained activation which could then potentially lead to exacerbated TNF-α signaling. Overall, these results point to a potential role of monocytes and DCs in the pathogenesis of MIS-C with severe myocarditis, which might not be directly driven by SARS-CoV-2 infection, but rather the consequence of a defect in a regulatory process limiting a pathological immune response, as already observed for other pathogens[43]. It would be interesting to investigate the presence of genetic variants among MIS-C with severe myocarditis, in genes such as *TNFAIP3,* as previously discussed[43]. The apparent hypoxic conditions detected in children with myocarditis, could also account for the exacerbation of NF-κB signaling. HIF-1α, a sensor of oxidative stress, is well-known for being able to induce a switch from oxidative phosphorylation to glycolysis to limit generation of reactive oxygen species (ROS). It can also activate NF-κB signaling[44,45]. Additional environmental factors and/or genetic predispositions could also be involved. Another striking feature was the low expression of genes involved in type-I and type-II interferon responses, specifically in

monocytes and DCs of children with myocarditis, although IFN-γ and IFN-α2 proteins were elevated in the plasma of all MIS-C patients. While an absence of type-II IFN responses could account for reduced HLA-DR cell surface expression by monocytes/DCs, the reduced response to type-I IFN in the most severe forms of MIS-C (with myocarditis and circulatory failure) is in part reminiscent of the impaired type-I IFN activity observed in the most severe forms of COVID-19 in adults[46–48]. The search for auto-antibodies against IFN-α2 were negative (data not shown) but presence of autoantibodies to interferon stimulated genes cannot be excluded[49]. As all MIS-C patients analyzed by SC-RNA-SEQ have received IVIG prior to sampling, the effect of the treatment is unlikely to explain the differences observed between MIS-C with or without severe myocarditis. Furthermore, IVIG has been described to downregulate rather than upregulate TNF-α and NF-κB signaling[24–26,29]. Of note, an abrogation of type-I IFN responses, following IVIG treatment has been described[50], although it is unlikely to explain here the differences between both groups of MIS-C.

Overall, our findings depict a model, supported by previous publications[51–53], in which myocarditis is associated with an attenuated negative feedback loop of TNF-α-driven NF-κB activation, together with an excess of proangiogenic cytokines and chemokines that could attract activated myeloid and T cells to the myocardium tissue (**Figure 7E**). Locally, it could lead to the production of inflammatory cytokines known to promote differentiation of cardiac fibroblasts into cardiac myofibroblasts (TNF-α, TGF-β, IL1β, IL-13, IL-4, VEGF). Cardiac myofibroblasts, as previously reported, may secrete chemokines leading to further activation and recruitment of myeloid cells, creating a feed-forward loop of locally sustained inflammation and myocarditis[51,54–57].

Using SC-RNA-SEQ data, we defined a gene signature specific of SARS-CoV-2-related postacute hyperinflammatory illness with severe myocarditis that was further validated by a global transcriptomic analysis on PBMCs from patients not analyzed by SC-RNA-SEQ. The

genes defining this signature were consistently enriched in genes associated with inflammation, TNF-α and NF-κB signaling, oxidative stress and myocarditis (**Figure S7C**). Interestingly, among these genes, the S100 proteins and the calprotectin complex (S100A8/S100A9) in particular, were previously reported and proposed as biomarkers for the most severe adult form of COVID-19 with acute respiratory syndrome (**Figure S7D**)[36]. Moreover, a recent deep immune profiling of adult and pediatric SARS-CoV-2 patients highlighted similarities between MIS-C and moderate to severe adult COVID-19 profiles[58]. Despite different clinical symptoms and disease temporality between adults infected with SARS-CoV-2 and children with MIS-C, our study underscored striking similarities at the cellular and molecular levels. Firstly, as observed in adults, increased leucocytes counts, activated neutrophils combined with lymphopenia, and decreased myeloid cells are characteristics of the most severe forms of MIS-C with myocarditis[17,41]. The hyper cytokinemia described in adults is also found in children with MIS-C (Elevated TNF-α, IL-6, IL-10, GM-CSF, monocyte chemoattractant protein 1 (MCP1)/CCL2, macrophage inflammatory protein (MIP-1α)/CCL3[36,59,60]. At the gene expression level, as reported in adults, the most severe disease forms in children are associated with TNF-α, NF-κB signaling, genes associated with hypoxia and/or oxidative stress (*HIF1A*; *HMGB1*) and reduced type-I IFN responses.

Interestingly, cardiac involvement in adult hospitalized patients with COVID-19 occurs frequently, with echocardiographic aspects similar to the pediatric MIS-C with myocarditis [61,62]. In some cases, they are associated with myocardial injury with dysfunction and elevated troponin levels, more often associated with poor outcomes[63–66]. In autopsy studies, cardiac infection was common in patients dying from COVID-19 although cells infected by SARS-CoV-2 were rare. Cardiac infection was often associated with myocardial inflammatory cell infiltration by macrophages and lymphocytes alongside myocarditis, in rare cases[67].

Limitations of the study

Our study has several limitations, including the relatively low number of cases in each group, the lack of a comparison with asymptomatic or mildly symptomatic non-hospitalized children positive for SARS-CoV-2 and a longitudinal study of children with “classic” KD enrolled before the COVID-19 pandemic. Our KD group was not homogeneous as it included both complete and incomplete KDs although we used the AHA algorithm and excluded other alternative diagnoses, we cannot exclude that incomplete KD cases were over-diagnosed and therefore misclassified. However, comparison of their biological and cytokine data with those of complete KD cases did not reveal any significant differences (data not shown), and we thought important to consider all KD cases that clinicians are confronted with in their daily practice. Also, due to the severity of the illness in MIS-C which requires immediate treatment, blood samples were almost exclusively collected post-immunomodulatory treatment by IVIG and in some cases following addition of glucocorticoids. Potential impacts of treatments were discussed throughout the manuscript. Differences in median age between groups exist and were taken into consideration during analyses. All our cellular data were generated from frozen peripheral mononuclear cells, which does not allow a direct assessment of neutrophils and cannot exclude any bias in cell proportions and immune analyses, although all samples were processed using the same methods. A parallel analysis of polymorphonuclear leukocytes will be required. Endothelial and myocardiac cells are at least targets of the disease but may also contribute to the pathophysiology as described above. Also, additional data supporting gene expression findings will be necessary in future studies. Nevertheless, our study provides further in-depth molecular analysis of MIS-C with severe myocarditis. These severe forms were found to be associated with an excessive activation of

481 the TNF-α, NF-κB signaling axis and poor response to type-I and type-II interferons in
482 monocytes and DCs, secretion of cytokines promoting angiogenesis, chemotaxis and
483 potential migration of activated myeloid cells and neutrophils in the myocardiac tissue. This
484 may help to identify potential new clinical biomarkers and open new therapeutic strategies,
485 including drugs targeting TNF-α or NF-κB pathways.
486

Consortium:

Pediatric-Biocovid Study Group: François Angoulvant, Camille Aupiais, Fanny Bajolle, Romain Basmaci, Paul Bastard, Matthieu Bendavid, Solène Blache, Stéphane Blanche, Christine Bodemer, Martin Chalumeau, Lucienne Chatenou, Anne Chauviré-Drouard, Fleur Cohen-Aubart, Agathe Debray, Albert Faye, Simon Fillatreau, Jacques Fourgeaud, Pierre Frange, Marion Grimaud, Lucile Houyel, Diala Khraiche, Hanane Kouider, Alain Lefevre-Utile, Pierre-Louis Leger, Morgane Le Gouez, Michael Levy, Manon Marchais, Soraya Matczak, Alexis Mathian, Bénédicte Neven, Perrine Parize, Olivier Pellé, Yael Pinhas, Marie Pouletty, Pierre Quartier dit Maire, Sylvain Renolleau, Anne-Sophie Romain, Laure de Saint-Blanquat, Isabelle Sermet, Melissa Taylor.

Acknowledgements:

The study was supported by the Institut National de la Santé et de la Recherche Médicale (INSERM), by the "URGENCE COVID-19" fundraising campaign of Institut Pasteur, by the Atip-Avenir, Emergence ville de Paris program and fond de dotation Janssen Horizon and by government grants managed by the Agence National de la Recherche as part of the "Investment for the Future" program (Institut Hospitalo-Universitaire Imagine, grant ANR-10-IAHU-01, Recherche Hospitalo-Universitaire, grant ANR-18-RHUS-0010, Laboratoire d'Excellence ''Milieu Intérieur", grant ANR-10-LABX-69-01), the Centre de Référence Déficits Immunitaires Héréditaires (CEREDIH), the Agence National de la Recherche (ANR-flash Covid19 "AIROCovid" to FRL and "CoVarImm" to DD and JDS), and by the FAST Foundation (French Friends of Sheba Tel Hashomer Hospital). The LabTech Single-Cell@Imagine is supported by the Paris Region and the "Investissements d'avenir" program through the 2019 ATF funding – Sésame Filières PIA (Grant N°3877871).

CdC is the recipient of a CIFRE-PhD (Sanofi). L.B. was a recipient of an Imagine institute PhD international program supported by the Fondation Bettencourt Schueller. L.B. was also supported by the EUR G.E.N.E. (reference #ANR-17-EURE-0013) and is part of the Université de Paris IdEx #ANR-18-IDEX-0001 funded by the French Government through its "Investments for the Future" program. S.M. was a recipient of an INSERM and Institut Imagine post-doctorat program supported by the Fondation pour la Recherche Médicale (FRM N°SPF20170938825). NS was a recipient of the Pasteur-Roux-Cantarini Fellowship. VGP obtained an Imagine international PhD fellowship program supported by the Fondation Bettencourt Schueller. BPP is the recipient of an ANRS post-doctoral fellowship. We thank

Imagine genomic, bioinformatic and single-cell core facilities, the Institut Pasteur Cytometry and Biomarkers UTechS platform and the Pitié-Salpêtrière Cytometry platform CyPS.

Author contributions:

CdC, ML, SM, AM, NS, FC, VGP, LB generated and analyzed data. MB, AB, BPP, GA, TF analyzed data. MB, LG, PG, JDS, HM, OS, CB, PB, and JLC generated data. CdC, ML, AF design figures and wrote manuscript. DD, FRL, JT and MMM conceived the study, analyzed data, wrote the manuscript, supervised the study and had unrestricted access to the data.

Declaration of interests:

DD, FRL, JT and MMM are listed as inventors on a patent application related to this technology (European Patent Application no. EP21305197, entitled “Methods of predicting multisystem inflammatory syndrome (MIS-C) with severe myocarditis in subjects suffering from a SARS-CoV-2 infection”).

Figure 1: Timeline and experimental designs. A. Timeline depicting when the different groups of pediatric patients were enrolled. **B.** Description of the different types of analyses performed on whole blood samples, peripheral blood mononuclear cells (PBMCs) and plasma. CyTOF: Mass cytometry (Cytometry by Time Of Flight). SC-RNA-SEQ: single-cell transcriptome sequencing. Bulk-RNA-SEQ: bulk level transcriptome sequencing. Simoa: Single molecule array, digital ELISA. Luminex: cytokine bead array assays. Ig dosage; quantification of SARS-CoV-2 specific immunoglobulins. CTL, healthy donors, green; *Acute-inf ($CoV2^-$)*, patients with acute respiratory infection but no evidence of SARS-CoV-2 infection, gray; *Acute-inf ($CoV2^+$)*, patients with acute respiratory infection and evidence of SARS-CoV-2 infection, blue; *MIS-C ($CoV2^+$)*, patients with postacute multi-inflammatory syndrome and evidence of SARS-CoV-2 infection, orange; *MIS-C_MYO ($CoV2^+$)*, patients with postacute hyperinflammatory syndrome, severe myocarditis and evidence of SARS-CoV-2 infection, red; *KD ($CoV2^-$)*, patients with postacute hyperinflammatory syndrome, no evidence of SARS-CoV-2 infection, but criteria for Kawasaki Disease (KD), pink. Illustrations were obtained from Servier Medical Art, licensed under a Creative Common Attribution 3.0 Generic License. http://smart.servier.com/. See also Figure S1 and Table S1.

Figure 2: Analyses of cytokine/chemokine plasma levels. A. Heatmap of all the cytokines/chemokines measured in the different clinical groups: CTL, green; *Acute-inf ($CoV2^+$)*, blue; *MIS-C ($CoV2^+$)*, orange; *MIS-C_MYO ($CoV2^+$),* red. On the x axis, blood donors are organized by groups and immune modulatory treatments (untreated, blue; treated, yellow) and on the y axis, cytokines/chemokines are displayed following hierarchical clustering. Cytokines/chemokines were expressed as pg/mL and log transformed with blue to orange colors representing lower to higher expression respectively. **B.** Dot plots of cytokines/chemokines elevated in postacute hyperinflammatory groups (*MIS-C ($CoV2^+$)*, *MIS-C_MYO ($CoV2^+$)*), as compared to *Acute-inf ($CoV2^+$)* and healthy blood donors (*CTL*). **C.** Dot plots of cytokines/chemokines elevated in *Acute-inf ($CoV2^+$)* as compared to postacute hyperinflammatory groups (*MIS-C ($CoV2^+$)*, *MIS-C_MYO ($CoV2^+$)*), and healthy blood donors (CTL). **B & C.** *P*-values are calculated by Kruskal-Wallis test for multiple comparisons, followed by a post-hoc Dunn's test. *($p < 0.05$), **($p < 0.01$), ***($p < 0.001$). See also Figure S2.

Figure 3: CyTOF and SC-RNA-SEQ characterization of PBMCs distribution. A. Upper panel: UMAP of 1,150,000 single cells from PBMCs of 7 CTL, 1 *Acute-inf (CoV2$^-$)*, 4 *Acute-inf (CoV2$^+$)*, 2 *MIS-C (CoV2$^+$)*, 6 *MIS-C_MYO (CoV2$^+$)* and 3 *KD (CoV2$^-$)* donors, following analyses by CyTOF and displayed as 23 clusters identified using the individual expression of 29 proteins, as described in Figure S3A. Bottom panel: boxplots of clusters with differences observed between SARS-CoV2$^+$ groups and CTL (*Acute-inf (CoV2$^+$)*, *MIS-C (CoV2$^+$)* and *MIS-C_MYO (CoV2$^+$)* **B.** Upper panel: UMAP of 152,201 single cells following extraction from PBMCs (9 CTL, 1 *Acute-inf (CoV2$^-$)*, 4 *Acute-inf (CoV2$^+$)*, 2 *MIS-C (CoV2$^+$)*, 6 *MIS-C_MYO (CoV2$^+$)*, and 3 *KD (CoV2$^-$)*) and processed by SC-RNA-SEQ. A resolution of 0.8 allows to segregate cells into 26 clusters identified based on the expression of several markers and gene signatures, as shown in Figure S4B. Bottom panel: Boxplots of clusters with significant differences between SARS-CoV2$^+$ groups and CTL (*Acute-inf (CoV2$^+$)*, *MIS-C (CoV2$^+$)* and *MIS-C_MYO (CoV2$^+$)*. See also Figure S3.
A & B. (CTL, green; *Acute-inf (CoV2$^+$)*, blue; *MIS-C (CoV2$^+$)*, orange; *MIS-C_MYO (CoV2$^+$)*). In the boxplots, each dot represents a sample. Boxes range from the 25th to the 75th percentiles. The upper and lower whiskers extend from the box to the largest and smallest values respectively. Any sample with a value at most x1.5 the inter-quartile range of the hinge is considered an outlier and plotted individually. *P*-values are calculated by Kruskal-Wallis test for multiple comparisons, followed by a post hoc Dunn's test. * ($p < 0.05$), **($p < 0.01$), ***($p < 0.001$).

Figure 4: Genes and pathways differentially regulated in acute infection and postacute hyperinflammation following SARS-CoV-2 infection. A. Bar charts of the number of up- and downregulated genes in *Acute-inf (CoV2$^+$)* (left panel) and All MIS-C (*MIS-C (CoV2$^+$)* and *MIS-C_MYO (CoV2$^+$)*) (right panel), compared to CTL, in PBMCs, monocytes/cDCs/pDCs, T and B cells clusters obtained following SC-RNA-SEQ experiments as displayed in Figure 3B. PBMCs represent all clusters; monocytes/cDCs/pDCs, clusters 5, 11, 12, 17, 20, 21, 24; T cells, clusters 0, 1, 2, 4, 6, 7, 10, 13, 14, 15, 16, 18, 23; and B cells, clusters 3, 8, 9, 19, and 22. The top value on the light-colored bars represents the upregulated genes and the bottom dark represents the downregulated genes. Median age for each group: CTL, 15 years; *MIS-C (CoV2$^+$)*, 3.7 years; *MIS-C_MYO (CoV2$^+$)*, 8.4 years **B.** Heatmap of the canonical pathways, enriched in the

differentially expressed genes (DEG) from the comparisons performed in A in PBMCs, monocytes/cDCs/pDCs, T and B cells, obtained by using Ingenuity Pathways Analysis (IPA). Left panel, part 1 and right panel part 2. Symbols are used in front to represent pathways of the same functional groups. Pathways with an absolute z-score ≤ 2 or adjusted *p*-value > 0.05 in all conditions were filtered out. Z-score > 2 means that a function is significantly increased (orange) whereas a Z-score < –2 indicates a significantly decreased function (blue). Grey dots indicate non-significant pathways (p > 0.05). **C.** Heatmap of the activation of NF-κB signaling pathway, as predicted by IPA, in *Acute-inf (CoV2$^+$)* and in All MIS-C (*MIS-C (CoV2$^+$)* and *MIS-C_MYO (CoV2$^+$)*) compared to controls. Color scale represents the z-score of the prediction. The higher the score, the more activated the NF-κB signaling pathway. "NS" means non-significant comparison. **D.** Dot plot of the expression in monocytes/cDCs/pDCs of the negative regulators of NF-κB complex. Color scale shows scaled average expression in all monocytes/cDCs/pDCs with red and blue being the highest and lowest expression respectively. Size of dot show the percentage of cells that express the gene. See also Figure S4 and supplementary file 2.

Figure 5: Cytokine/chemokine and gene expression analyses reveal an exacerbation of TNF-α and NF-κB signaling pathways in MIS-C_MYO (CoV2$^+$) as compared to MIS-C (CoV2$^+$). A. Heatmap of the cytokines/chemokines showing differences between *MIS-C (CoV2$^+$)*, orange and *MIS-C_MYO (CoV2$^+$),* red, in patients not treated by corticosteroids before sampling. On the x axis, blood donors are organized by groups and treatments received before sampling. On the y axis, cytokines/chemokines are displayed following hierarchical clustering. Cytokines/chemokines were expressed as pg/mL and log transformed with blue to orange colors representing lower to higher expression respectively. **B.** Dot plots of cytokines/chemokines elevated *MIS-C_MYO (CoV2$^+$)* as compared to *MIS-C (CoV2$^+$)* and related to TNF-α and NF-κB signaling. *P*-values are calculated by Kruskall-Wallis test for multiple comparisons, followed by a post hoc Dunn's test. *($p < 0.05$), **($p < 0.01$), ***($p < 0.001$). **C.** Dot plot of the expression in monocytes/cDCs/pDCs of the 49 genes from the TNF-α signaling via NF-κB pathway (pathway enrichment analysis by MSigDB Hallmark 2020 obtained from the upregulated genes of in the *MIS-C_MYO (CoV2$^+$)* group compared to *MIS-C (CoV2$^+$)* (Figure S6B)). **D.** Dot plot of the expression in monocytes/cDCs/pDCs of the negative regulators of NF-κB complex in the MIS-C groups. See also Figure S5 and supplementary file 2.

Figure 6: Differences in Interferon responses between *MIS-C (CoV2$^+$)* and *MIS-C_MYO (CoV2$^+$)*. **A.** IFN-α and IFN-γ protein levels measured by Simoa (top two panels) and IFN-stimulated genes (Type-I and Type-II ISGs) expression measured by SC-RNA-SEQ and displayed as signature score on all PBMCs (bottom two panels) **B & C.** Violin plots of Type-I (B) and Type-II (C) interferon signaling signatures analyzed in monocytes/cDCs/pDCs, B and T cells. **D.** Dot plot of the expression in monocytes/cDCs/pDCs cells of 60 genes from the Interferon signaling pathway enrichment analysis by MSigDB Hallmark 2020 obtained from the downregulated genes of in the *MIS-C_MYO (CoV2$^+$)* group compared to *MIS-C (CoV2$^+$)* (Figure S6E). See also Figure S6.

A & D. Color scale shows scaled average expression in all cells with red and blue being the highest and lowest expression respectively. Size of dot show the percentage of cells that express the gene.

Figure 7: Molecular signature and proposed mechanism associated with severe myocarditis in children with MIS-C. A. Schematic representation of the 3 strategies used to extract 329 markers of the *MIS-C_MYO (CoV2$^+$)* group from the monocytes/cDCs/pDCs clusters using the single-cell dataset. Strategy 1: direct comparison of the monocytes/cDCs/pDCs cells of the *MIS-C_MYO (CoV2$^+$)* group to all other samples. Strategy 2: direct comparison of the monocytes/cDCs/pDCs cells of *MIS-C_MYO (CoV2$^+$)* to other samples with postacute hyperinflammation (*MIS-C (CoV2$^+$)* and *KD (CoV2$^-$)*). Strategy 3: selection of the genes upregulated only in the monocytes/cDCs/pDCs of *MIS-C_MYO (CoV2$^+$)* when compared to CTL. Below each strategy, the corresponding dot plot obtained from SC-RNA-SEQ, with the number of upregulated genes. The average expression is represented by the centered scaled expression of each gene. On the left, names of each group with its corresponding color is shown. **B.** Heatmap of the expression of the 116/329 genes with a higher expression in *MIS-C_MYO (CoV2$^+$)* than in other groups in the bulk dataset (7 CTL, 7 *MIS-C (CoV2$^+$)*, 9 *MIS-C_MYO (CoV2$^+$)* and 9 *KD (CoV2$^-$)* donors). Color scale indicates the scaled GeneSCORE (mean z-score of the gene in all samples of a group), with red and blue representing the highest and lowest expressions respectively. Hierarchical clustering of the genes was computed with a Pearson's correlation as a distance. **C.** Box plot of the expression of the 116 genes validated in C, calculated as a SignatureScore, which represents the mean z-score in each sample of the 116 genes selected in B in the bulk-

RNA-SEQ dataset (see Figure S7A). **D.** Boxplot of the SignatureScore of the top 25 genes, as ranked in Figure S7B, in the Bulk-RNA-SEQ dataset. **E.** Graphical representation based on cytokines, cellular and transcriptomic analyses (part above black dotted line), combined with known literature (part under the black dotted line), illustrating a putative model explaining the occurrence of myocarditis among children in the MIS-C (CoV2) group. Black writing represents genes and functions both modulated in the *MIS-C ($CoV2^+$)* and *MIS-C_MYO ($CoV2^+$)* groups compared to CTL, whereas red highlights genes and pathways differentially modulated in the *MIS-C ($CoV2^+$)* and *MIS-C_MYO ($CoV2^+$)* groups, respectively. See also Figure S7 and supplementary file 3.

C & D. Each mark represents a sample. Dots are untreated samples, triangles are IVIG-treated samples, squares are IVIG and steroids-treated patients. Boxes range from the 25th to the 75th percentiles. The upper and lower whiskers extend from the box to the largest and smallest values respectively. Any sample with a value at most x1.5 the inter-quartile range of the hinge is considered an outlier and plotted individually.

Resource Availability

Lead Contact

Further information and requests for resources and reagents should be directed to and will be fulfilled by the Lead Contact and corresponding author, Mickaël Ménager (mickael.menager@institutimagine.org)

Material availability

This study did not generate new unique reagents.

Data and Code availability

Single-cell and bulk RNA-seq data have been deposited in GEO and are publicly available. Accession numbers are listed in the key resources table. This paper does not report original code. Any additional information required to reanalyze the data reported in this paper is available from the lead contact upon request. Additional Supplemental Items are available from Mendeley Data at http://dx.doi.org/10.17632/wm4z48cftc.1

Experimental Model and Subject details

Patients and cohorts

This prospective multicenter cohort study included children (age ≤ 18 years at the time of admission) suspected of infection with SARS-CoV-2 between April 6, 2020 and May 30, 2020. Clinical aspects of 22 of the included patients were previously reported[10,11]. Children admitted with fever in general pediatric wards or pediatric intensive care units of Tertiary French hospitals involved in the research program, suspected of SARS-CoV-2 related illness and who underwent routine nasopharyngeal swabs for SARS-CoV-2 RT-PCR (R-GENE, Argene, Biomerieux, Marcy l'Etoile) or SARS-CoV-2 IgG serology testing (Architect SARS-CoV-2 chemiluminescent microparticle immunoassay; Abbott Core Laboratory, IL, USA), were eligible. The study was approved by the Ethics Committee (Comité de Protection des Personnes Ouest IV, n° DC-2017-2987). All parents provided written informed consent.

Case definition for pediatric COVID-19 acute infection was presence of fever, fatigue, neurological abnormalities, gastro-intestinal or respiratory signs, associated with a concomitant nasopharyngeal swab positive for SARS-CoV-2 RT-PCR, and absence of MIS-C criteria[68]. Case definition for postacute hyperinflammatory illness (**Figure 1**) was presence of fever, laboratory evidence of inflammation and clinically severe illness with multisystem involvement, during the SARS-CoV-2 epidemic period[7]. This may include children with features of KD; criteria of the American Heart Association was used to define for complete (Fever > 4 days and ≥ 4 principal criteria) or incomplete KD (Fever > 4 days and 2 or 3 principal criteria, and without characteristics suggestive of another diagnosis)[13]. Among cases with postacute hyperinflammatory illness, children with a positive SARS-CoV-2 testing (RT-PCR or serology) were considered to have MIS-C according to CDC and WHO criteria to define MIS-C[69]. Patients with postacute hyperinflammatory illness, negative SARS-CoV-2 testing (RT-PCR or serology), and criteria for KD, were considered as patients with KD-like illness. Patients with MIS-C with clinical signs of circulatory failure requiring intensive care, with elevated high-sensitivity cardiac troponin I levels (>26 ng/mL) and/or decreased cardiac function (diastolic or systolic ventricular dysfunction at echocardiography), were considered to have MIS-C with severe myocarditis[70,71].

For each included patient, we collected demographic data, symptoms, results of SARS-CoV-2 testing and other laboratory tests, echocardiograms, and treatments. All patient data are available in Supplementary Table 1. Introduction of specific treatments for MISC and KD cases was decided by the pediatrician in charge of the patient; it generally consisted of intravenous polyvalent immunoglobulins [IVIG] alone (2g/kg in one or two infusions), or IVIG associated with methylprednisolone (2-10 mg/kg/day for at least 3 days) as first or second-line therapy. Patients with negative initial serology testing were retested after an

interval of at least 3 weeks (Architect SARS-CoV-2 chemiluminescent microparticle immunoassay; Abbott Core Laboratory).

Healthy controls were recruited before the COVID-19 pandemic (before November 2019).

Samples

For each patient and healthy donor, peripheral blood samples were collected on EDTA and lithium heparin tubes. After a centrifugation of the EDTA tube at 2300rpm for 10 minutes, plasma was taken and stored at −80°C before cytokine quantification. PBMCs were isolated from the lithium heparin samples, frozen as described below and stored at −80°C and were used for both bulk and single-cell RNAseq, as well as cell phenotyping by CyTOF. The number of samples included in each dataset is summarized in the metadata table (Supp1_Metadata) and the workflow is summarized in Figure 1B.

Methods details

Isolation of PBMCs

Peripheral blood samples were collected on lithium heparin. PBMCs were isolated by density gradient centrifugation (2,200 rpm without break for 30 minutes) using Ficoll (Eurobio Scientific, Les Ulis, France). After centrifugation, cells were washed with Phosphate-buffered saline (PBS) (Thermo Fisher scientific, Illkirch, France). The pellet was resuspended in PBS and cells were centrifuged at 1,900 rpm for 5 minutes. Finally, the PBMCs pellet was frozen in a medium containing 90% of Fetal Bovine Serum (FBS) (Gibco, Thermo Fisher scientific, Illkirch, France) and 10% of dimethyl sulfoxide (DMSO) (Sigma Aldrich, St. Quentin Fallavier, France).

Cytokine measurements

Prior to protein analysis plasma samples were treated in a BSL3 laboratory for viral decontamination using a protocol previously described for SARS-CoV[72], which we validated for SARS-CoV-2. Briefly, samples were treated with TRITON X100 (TX100) 1% (v/v) for 2h at Room Temperature. IFN-α2, IFN-γ, IL-17A, (triplex) and IFN-β (single plex) protein plasma concentrations were quantified by Simoa assays developed with Quanterix Homebrew kits as previously described [73]. The limit of detection of these assays were 0.6 pg/mL for IFN-β, 2 fg/mL for IFN-α2, 0.05 pg/ml for IFN-γ and 3 pg/mL for IL-17A including the dilution factor. IL-6, TNF-α, and IL-10 were measured with a commercial triplex assay (Quanterix). Additional plasma cytokines and chemokines (44 analytes) were measured with a commercial Luminex multi-analyte assay (Biotechne, R&D systems).

Serology assays

SARS-CoV-2 specific antibodies were quantified using assays previously described[74]. Briefly, a standard ELISA assay using as target antigens the extracellular domain of the S protein in the form of a trimer (ELISA tri-S) and the S-Flow assay, which is based on the recognition of SARS-CoV-2 S protein expressed on the surface of 293T cells (293T-S), were used to quantify SARS-CoV-2 specific IgG and IgA subtypes in plasma. Assay characteristics including sensitivity and specificity were previously described[74].

Cell Phenotyping

To perform high-dimensional immune profiling of PBMCs, we used the Maxpar® Direct™ Immune Profiling System (Fluidigm, Inc France) with a 30-marker antibody panel, for CyTOF (Cytometry by Time Of Flight). Briefly, $3x10^6$ PBMCs resuspended in 300 µl of

MaxPar Cell Staining Buffer were incubated for 20 minutes at room temperature after addition of 3 µL of 10 KU/mL heparin solution and 5 µl of Human TruStain FcX (Biolegend Europ, Netherland). Then 270 µL of the samples were directly added to the dry antibody cocktail for 30 minutes. 3 mL of MaxPar Water was added to each tube for an additional 10-min incubation. Three washes were performed on all the samples using MaxPar Cell Staining Buffer and they were fixed using 1.6% paraformaldehyde (Sigma-Aldrich, France). After one wash with MaxPar Cell Staining Buffer, cells were incubated one hour in Fix and Perm Buffer with 1:1,000 of Iridium intercalator (pentamethylcyclopentadienyl-Ir (III)-dipyridophenazine, Fluidigm, Inc France). Cells were washed and resuspended at a concentration of 1 million cells per mL in Maxpar Cell Acquisition Solution, a high-ionic-strength solution, and mixed with 10% of EQ Beads immediately before acquisition.

Acquisition of the events was made on the Helios mass cytometer and CyTOF software version 6.7.1014 (Fluidigm, Inc Canada) at the "Plateforme de Cytométrie de la Pitié-Salpetriere (CyPS)." An average of 500,000 events were acquired per sample. Dual count calibration, noise reduction, cell length threshold between 10 and 150 pushes, and a lower convolution threshold equal to 10 were applied during acquisition. Mass cytometry standard files produced by the HELIOS were normalized using the CyTOF Software v. 6.7.1014. For data cleaning, 4 parameters (centre, offset, residual and width) are used to resolve ion fusion events (doublets) from single events from the Gaussian distribution generated by each event[75]. After data cleaning, the program produces new FCS files consisting of only intact live singlet cells. These data were analyzed in FlowJo v10.7.1 using 3 plugins (DownSampleV3, UMAP and FlowSOM) with R v4.0.2. To increase efficiency of the analysis, samples were downsampled to 50,000 cells, using the DownSample V3 plugin. All samples were concatenated and analyzed in an unsupervised manner. Anti-CD127 antibody had to be excluded due to poor staining. Clustering was performed using FlowSOM[76]. The

number of clusters was set to forty-five in order to overestimate the populations and detect smaller subpopulations. Grid size of the self-organizing map was set to 20x20. Resulting clusters were annotated as cell populations following the kit manufacturer's instruction. When several clusters were identified as the same cell types, they were concatenated into a single cell population. For visualization purposes, UMAP was computed with the UMAP pluggin[77] with the following parameters: metric (Euclidean), nearest neighbors (15), minimum distance (0.5) and number of components (2).

Single-cell transcriptomic (SC-RNA-SEQ)

SC-RNA-SEQ analyses were performed on frozen PBMCs isolated from heparin blood samples. PBMCs were thawed according to 10X Genomics protocol. The SC-RNA-SEQ libraries were generated using Chromium Single Cell 3′ Library & Gel Bead Kit v.3 (10x Genomics) according to the manufacturer's protocol. Briefly, cells were counted, diluted at 1,000 cells/µL in PBS+0.04% and 20,000 cells were loaded in the 10x Chromium Controller to generate single-cell gel-beads in emulsion. After reverse transcription, gel-beads in emulsion were disrupted. Barcoded complementary DNA was isolated and amplified by PCR. Following fragmentation, end repair and A-tailing, sample indexes were added during index PCR. The purified libraries were sequenced on a Novaseq 6000 (Illumina) with 28 cycles of read 1, 8 cycles of i7 index and 91 cycles of read 2.

Sequencing reads were demultiplexed and aligned to the human reference genome (GRCh38, release 98, built from Ensembl sources), using the CellRanger Pipeline v3.1. Unfiltered RNA UMI counts were loaded into Seurat v3.1[78] for quality control, data integration and downstream analyses. Apoptotic cells and empty sequencing capsules were excluded by filtering out cells with fewer than 500 features or a mitochondrial content higher than 20%. Data from each sample were log-normalized and scaled, before batch correction using

Seurat's FindIntegratedAnchors. For computational efficiency, anchors for integration were determined using all control samples as reference and patient samples were projected onto the integrated controls space. On this integrated dataset, we computed the principal component analysis on the 2000 most variable genes. UMAP was carried out using the 20 most significant principal components (PCs), and community detection was performed using the graph-based modularity-optimization Louvain algorithm from Seurat's FindClusters function with a 0.8 resolution. Cell types labels were assigned to resulting clusters based on a manually curated list of marker genes as well as previously defined signatures of the well-known PBMCs subtypes[79]. Despite filtering for high quality cells, five clusters out of the twenty-six stood out as poor quality clusters and were removed from further analysis, namely: one erythroid-cell contamination; one low UMI cluster from a single control; two clusters of proliferating cells originating from a patient with EBV co-infection and one megakaryocytes cluster. In total 152,201 cells were kept for further analysis.

After extraction and reclustering of high-quality cells, differential expression was performed separately on all PBMCs, monocytes/DCs, T cells or B cells. Differential expression testing was conducted using the FindMarkers function of Seurat on the RNA assay with default parameters. Genes with log(FC) > 0.25 and adjusted *p*-values $\leq$0.05 were selected as significant. Differential analysis results and links to the pathways analysis in EnrichR[34,35] can be found in supplementary file 2. Transcriptomic signatures for Type-I and Type-II interferon signaling were performed using Seurat's AddModuleScore function, based on interferon-stimulated gene lists extracted from Rosenberg, *et al.*[80] and Reactome database respectively. Violin plots were performed using Seurat's VlnPlot function.

Bulk RNA-sequencing (Bulk-RNA-SEQ)

Bulk-RNA-SEQ analyses were performed on frozen PBMCs extracted from heparin samples. RNA was extracted from PBMCs following the instructions of RNeasyR Mini kit (Qiagen, Courtaboeuf, France). To note, the optional step with the DNase was performed. RNA integrity and concentration were assessed by capillary electrophoresis using Fragment Analyzer (Agilent Technologies). RNAseq libraries were prepared starting from 100 ng of total RNA using the Universal Plus mRNA-Seq kit (Nugen) as recommended by the manufacturer. The oriented cDNA produced from the poly-A+ fraction was sequenced on a NovaSeq6000 from Illumina (Paired-End reads 100 bases + 100 bases). A total of ~50 million of passing-filters paired-end reads was produced per library.

Paired-end RNA-seq reads were aligned to the human Ensembl genome GRCh38.91 using Hisat2 (v2.0.4)[81] and counted using featureCounts from the Subread R package. The raw count matrix was analyzed using DESeq2 (version 1.28.1)[82]. No pre-filtering was applied to the data. Differential expression analysis was performed using the "DESeq" function with default parameters. For visualization and clustering, the data was normalized using the `variant stabilizing transformation` method implemented in the “vst” function. Plots were generated using ggplot2 (version 3.3.2), and pheatmap (version 1.0.12).

During exploratory analyses, it was noted that the clustering was mainly driven by the sex of the patients. To remove this effect, it was included in the regression formula for DESeq (~sex + groups), and then removed following vst transformation, using "removeBatchEffect" from the "limma" package (version 3.44.3).

Gene signature analysis

To identify genes that could be used as markers of severe myocarditis in the SC-RNA-SEQ dataset, three initial strategies were used, all based on differential expression and selection of the upregulated genes. First, we performed the differential expression between *MIS-C_MYO*

(CoV2⁺) samples and all other samples. Second, differential analysis was computed between *MIS-C_MYO (CoV2⁺)* and other samples with postacute hyperinflammatory illness. In the last strategy, we selected genes that were upregulated between the *MIS-C_MYO (CoV2⁺)* and the CTL, but not upregulated in any other group compared to the CTL (Figure 7A). These three strategies allowed us to identify 329 unique genes.

To further explore whether these genes could be considered as markers of severe myocarditis, we analyzed their expression profile in our bulk RNA-SEQ dataset. This dataset excluded samples from patients of the *MIS-C_MYO (CoV2⁺)* that were included in the SC-RNA-SEQ cohort. Vst-transformed counts were log2-normalized and converted to z-score using the scale function in R (v 4.0.2). A GeneSCORE was computed for each group as the mean z-score of the samples of a group. Heatmaps representing this $\text{GeneSCORE}_{\text{group}}$ were performed using pheatmap. Hierarchical clustering of the 329 previously identified genes was performed using the complete method on the distance measured using Pearson's correlation, as implemented by pheatmap. The hierarchical clustering was divided into 15 main clusters, 4 of which had the expected pattern of expression: Clusters that had a higher expression in *MIS-C_MYO (CoV2⁺)* than any other group were selected, resulting in 116 genes. A signature score for each sample was performed on these genes, corresponding to the mean expression (z-score) of these N genes in each sample (SignatureSCORE).

These genes were subsequently ranked based on the following equation:

$$RankingSCORE = GeneSCORE_{MIS-C\_MYO\ (CoV2+)} - (GeneSCORE_{MIS-C\ (CoV2+)} + GeneSCORE_{KD\ (CoV2-)})$$

where the SCOREs represent the mean expression (z-score) in each disease groups, and the SignatureScore was computed on the top 25 genes. All gene lists and scores can be found in supplementary file 3.

Quantification and statistical analysis

Cytokine heatmaps were made with Qlucore OMICS explore (version 3.5(26)) and dot plots with GraphPad Prism (version 8). Differentially secreted cytokines were included in the heat maps based on a 1.5-Fold Change (FC) comparison between groups as indicated. Dot plot differences between each group were identified by Kruskal-Wallis tests followed by post-hoc multiple comparison Dunn's test.

Statistical tests for cellular composition analysis in both the CyTOF and SC-RNA-SEQ datasets were performed in R v3.6.1. Kruskal-Wallis test followed by post-hoc multiple comparison Dunn's test was applied to assess differences in cell population proportions (*: $p \leq 0.05$; **: $p \leq 0.01$; ***: $p \leq 0.001$).

Differential expression testing in the SC-RNA-SEQ dataset was conducted using the FindMarkers function in Seurat, with default Wilcoxon testing. *P*-values were controlled using Bonferroni correction. Genes with an absolute log(fold-change) ≥0.25 and an adjusted *p*-value ≤0.05 were selected as differentially expressed. Pathways analysis was performed using both the Ingenuity pathway analysis v57662101 software (IPA (QIAGEN Inc.) and EnrichR[34,35]. Heatmaps were extracted from the comparison module in IPA. Pathways with an absolute z-score lower than 2 or a Bonferroni-Hochberg corrected *p*-values higher than 0.05 were filtered out. Reactome 2016 and Molecular Signature DataBase Hallmark 2020 (MSigDB Hallmark 2020) pathway enrichment analysis was performed using EnrichR. The TRRUST transcription factors 2019[21] used for the transcription factors enrichment analysis was performed using Enrich R. All differential analysis performed and the links to the EnrichR results are indicated in supplementary file 2.

Supplementary file 1: Metadata table indicating samples from patients and healthy controls included in each analysis. Related to Figure 1, Figure S1.

Supplementary file 2:

Tables of differentially expressed genes and EnrichR links. Related to Related to Figure 4, Figure S4, and Figure S5.

This spreadsheet includes the differential expression tables for all comparisons presented in the paper, performed on all PBMCs and on major cell types (monocytes/cDCs/pDCs, T cells, or B cells). Links to EnrichR analysis presented in Figure S6 are included.

Supplementary file 3:

Tables of differentially expressed genes and of the different scores generated. Related to Figure 7 and Figure S7.

The list of genes extracted from SC-RNA-seq data coming from the 3 different strategies used are listed, alongside the different scores generated from Bulk-RNA-seq data.

References

1. Wiersinga, W.J., Rhodes, A., Cheng, A.C., Peacock, S.J., and Prescott, H.C. (2020). Pathophysiology, Transmission, Diagnosis, and Treatment of Coronavirus Disease 2019 (COVID-19): A Review. JAMA *324*, 782–793.

2. Brodin, P. (2020). Why is COVID-19 so mild in children? Acta Paediatr *109*, 1082–1083.

3. Castagnoli, R., Votto, M., Licari, A., Brambilla, I., Bruno, R., Perlini, S., Rovida, F., Baldanti, F., and Marseglia, G.L. (2020). Severe Acute Respiratory Syndrome Coronavirus 2 (SARS-CoV-2) Infection in Children and Adolescents: A Systematic Review. JAMA Pediatr *174*, 882–889.

4. Gudbjartsson, D.F., Helgason, A., Jonsson, H., Magnusson, O.T., Melsted, P., Norddahl, G.L., Saemundsdottir, J., Sigurdsson, A., Sulem, P., Agustsdottir, A.B., et al. (2020). Spread of SARS-CoV-2 in the Icelandic Population. N Engl J Med *382*, 2302–2315.

5. Levy, C., Basmaci, R., Bensaid, P., Bru, C.B., Coinde, E., Dessioux, E., Fournial, C., Gashignard, J., Haas, H., Hentgen, V., et al. (2020). Changes in RT-PCR-positive SARS-CoV-2 rates in adults and children according to the epidemic stages. medRxiv, 2020.05.18.20098863.

6. Tagarro, A., Epalza, C., Santos, M., Sanz-Santaeufemia, F.J., Otheo, E., Moraleda, C., and Calvo, C. (2020). Screening and Severity of Coronavirus Disease 2019 (COVID-19) in Children in Madrid, Spain. JAMA Pediatr.

7. Datta, S.D., Talwar, A., and Lee, J.T. (2020). A Proposed Framework and Timeline of the Spectrum of Disease Due to SARS-CoV-2 Infection: Illness Beyond Acute Infection and Public Health Implications. JAMA *324*, 2251–2252.

8. Abrams, J.Y., Godfred-Cato, S.E., Oster, M.E., Chow, E.J., Koumans, E.H., Bryant, B., Leung, J.W., and Belay, E.D. (2020). Multisystem Inflammatory Syndrome in Children Associated with Severe Acute Respiratory Syndrome Coronavirus 2: A Systematic Review. J Pediatr *226*, 45-54.e1.

9. Jones, V.G., Mills, M., Suarez, D., Hogan, C.A., Yeh, D., Segal, J.B., Nguyen, E.L., Barsh, G.R., Maskatia, S., and Mathew, R. (2020). COVID-19 and Kawasaki Disease: Novel Virus and Novel Case. Hosp Pediatr *10*, 537–540.

10. Toubiana, J., Poirault, C., Corsia, A., Bajolle, F., Fourgeaud, J., Angoulvant, F., Debray, A., Basmaci, R., Salvador, E., Biscardi, S., et al. (2020). Kawasaki-like multisystem inflammatory syndrome in children during the covid-19 pandemic in Paris, France: prospective observational study. BMJ *369*, m2094.

11. Toubiana, J., Cohen, J.F., Brice, J., Poirault, C., Bajolle, F., Curtis, W., Moulin, F., Matczak, S., Leruez, M., Casanova, J.-L., et al. (2021). Distinctive Features of Kawasaki Disease Following SARS-CoV-2 Infection: a Controlled Study in Paris, France. J Clin Immunol.

12. Whittaker, E., Bamford, A., Kenny, J., Kaforou, M., Jones, C.E., Shah, P., Ramnarayan, P., Fraisse, A., Miller, O., Davies, P., et al. (2020). Clinical Characteristics of 58 Children With a Pediatric Inflammatory Multisystem Syndrome Temporally Associated With SARS-CoV-2. JAMA *324*, 259–269.

13. McCrindle, B.W., Rowley, A.H., Newburger, J.W., Burns, J.C., Bolger, A.F., Gewitz, M., Baker, A.L., Jackson, M.A., Takahashi, M., Shah, P.B., et al. (2017). Diagnosis, Treatment, and Long-Term Management of Kawasaki Disease: A Scientific Statement for Health Professionals From the American Heart Association. Circulation *135*, e927–e999.

14. Kanegaye, J.T., Wilder, M.S., Molkara, D., Frazer, J.R., Pancheri, J., Tremoulet, A.H., Watson, V.E., Best, B.M., and Burns, J.C. (2009). Recognition of a Kawasaki disease shock syndrome. Pediatrics *123*, e783-789.

15. Turnier, J.L., Anderson, M.S., Heizer, H.R., Jone, P.-N., Glodé, M.P., and Dominguez, S.R. (2015). Concurrent Respiratory Viruses and Kawasaki Disease. Pediatrics *136*, e609-614.

16. Carter, M.J., Fish, M., Jennings, A., Doores, K.J., Wellman, P., Seow, J., Acors, S., Graham, C., Timms, E., Kenny, J., et al. (2020). Peripheral immunophenotypes in children with multisystem inflammatory syndrome associated with SARS-CoV-2 infection. Nature Medicine *26*, 1701–1707.

17. Consiglio, C.R., Cotugno, N., Sardh, F., Pou, C., Amodio, D., Rodriguez, L., Tan, Z., Zicari, S., Ruggiero, A., Pascucci, G.R., et al. (2020). The Immunology of Multisystem Inflammatory Syndrome in Children with COVID-19. Cell *183*, 968-981.e7.

18. Gruber, C.N., Patel, R.S., Trachtman, R., Lepow, L., Amanat, F., Krammer, F., Wilson, K.M., Onel, K., Geanon, D., Tuballes, K., et al. (2020). Mapping Systemic Inflammation and Antibody Responses in Multisystem Inflammatory Syndrome in Children (MIS-C). Cell *183*, 982-995.e14.

19. Cheng, M.H., Zhang, S., Porritt, R.A., Rivas, M.N., Paschold, L., Willscher, E., Binder, M., Arditi, M., and Bahar, I. (2020). Superantigenic character of an insert unique to SARS-CoV-2 spike supported by skewed TCR repertoire in patients with hyperinflammation. PNAS *117*, 25254–25262.

20. Kobayashi, T., Inoue, Y., Takeuchi, K., Okada, Y., Tamura, K., Tomomasa, T., Kobayashi, T., and Morikawa, A. (2006). Prediction of intravenous immunoglobulin unresponsiveness in patients with Kawasaki disease. Circulation *113*, 2606–2612.

21. Han, H., Cho, J.-W., Lee, S., Yun, A., Kim, H., Bae, D., Yang, S., Kim, C.Y., Lee, M., Kim, E., et al. (2018). TRRUST v2: an expanded reference database of human and mouse transcriptional regulatory interactions. Nucleic Acids Res *46*, D380–D386.

22. Séïté, J.-F., Hillion, S., Harbonnier, T., and Pers, J.-O. (2015). Review: Intravenous Immunoglobulin and B Cells: When the Product Regulates the Producer. Arthritis & Rheumatology *67*, 595–603.

23. Bayry, J., Lacroix-Desmazes, S., Carbonneil, C., Misra, N., Donkova, V., Pashov, A., Chevailler, A., Mouthon, L., Weill, B., Bruneval, P., et al. (2003). Inhibition of maturation and function of dendritic cells by intravenous immunoglobulin. Blood *101*, 758–765.

24. Das, M., Karnam, A., Stephen-Victor, E., Gilardin, L., Bhatt, B., Kumar Sharma, V., Rambabu, N., Patil, V., Lecerf, M., Käsermann, F., et al. (2020). Intravenous immunoglobulin mediates anti-inflammatory effects in peripheral blood mononuclear cells by inducing autophagy. Cell Death & Disease *11*, 1–14.

25. Galeotti, C., Kaveri, S.V., and Bayry, J. (2017). IVIG-mediated effector functions in autoimmune and inflammatory diseases. International Immunology *29*, 491–498.

26. Kozicky, L.K., Menzies, S.C., Zhao, Z.Y., Vira, T., Harnden, K., Safari, K., Del Bel, K.L., Turvey, S.E., and Sly, L.M. (2018). IVIg and LPS Co-stimulation Induces IL-10 Production by Human Monocytes, Which Is Compromised by an FcγRIIA Disease-Associated Gene Variant. Front Immunol *9*.

27. Cicha, A., Fischer, M.B., Wesinger, A., Haas, S., Bauer, W.M., Wolf, H.M., Sauerwein, K.M.T., Reininger, B., Petzelbauer, P., Pehamberger, H., et al. (2018). Effect of intravenous immunoglobulin administration on erythrocyte and leucocyte parameters. Journal of the European Academy of Dermatology and Venereology *32*, 1004–1010.

28. Dyer, W.B., Tan, J.C.G., Day, T., Kiers, L., Kiernan, M.C., Yiannikas, C., Reddel, S., Ng, K., Mondy, P., Dennington, P.M., et al. (2016). Immunomodulation of inflammatory leukocyte markers during intravenous immunoglobulin treatment associated with clinical efficacy in chronic inflammatory demyelinating polyradiculoneuropathy. Brain Behav *6*.

29. Schwab, I., and Nimmerjahn, F. (2013). Intravenous immunoglobulin therapy: how does IgG modulate the immune system? Nat Rev Immunol *13*, 176–189.

30. Tha-In, T., Metselaar, H.J., Tilanus, H.W., Boor, P.P.C., Mancham, S., Kuipers, E.J., de Man, R.A., and Kwekkeboom, J. (2006). Superior Immunomodulatory Effects of Intravenous Immunoglobulins on Human T-cells and Dendritic Cells: Comparison to Calcineurin Inhibitors. Transplantation *81*, 1725–1734.

31. Tha-In, T., Metselaar, H.J., Tilanus, H.W., Groothuismink, Z.M.A., Kuipers, E.J., de Man, R.A., and Kwekkeboom, J. (2007). Intravenous immunoglobulins suppress T-cell priming by modulating the bidirectional interaction between dendritic cells and natural killer cells. Blood *110*, 3253–3262.

32. Holbrook, J., Lara-Reyna, S., Jarosz-Griffiths, H., and McDermott, M.F. (2019). Tumour necrosis factor signalling in health and disease. F1000Res *8*.

33. Varfolomeev, E.E., and Ashkenazi, A. (2004). Tumor Necrosis Factor: An Apoptosis JuNKie? Cell *116*, 491–497.

34. Chen, E.Y., Tan, C.M., Kou, Y., Duan, Q., Wang, Z., Meirelles, G.V., Clark, N.R., and Ma'ayan, A. (2013). Enrichr: interactive and collaborative HTML5 gene list enrichment analysis tool. BMC Bioinformatics *14*, 128.

35. Kuleshov, M.V., Jones, M.R., Rouillard, A.D., Fernandez, N.F., Duan, Q., Wang, Z., Koplev, S., Jenkins, S.L., Jagodnik, K.M., Lachmann, A., et al. (2016). Enrichr: a comprehensive gene set enrichment analysis web server 2016 update. Nucleic Acids Res *44*, W90-97.

36. Silvin, A., Chapuis, N., Dunsmore, G., Goubet, A.-G., Dubuisson, A., Derosa, L., Almire, C., Hénon, C., Kosmider, O., Droin, N., et al. (2020). Elevated Calprotectin and Abnormal Myeloid Cell Subsets Discriminate Severe from Mild COVID-19. Cell *182*, 1401-1418.e18.

37. Kunkel, S.L., Standiford, T., Kasahara, K., and Strieter, R.M. (1991). Interleukin-8 (IL-8): the major neutrophil chemotactic factor in the lung. Exp Lung Res *17*, 17–23.

38. Pease, J.E., and Sabroe, I. (2002). The Role of Interleukin-8 and its Receptors in Inflammatory Lung Disease. Am J Respir Med *1*, 19–25.

39. Sawant, K.V., Xu, R., Cox, R., Hawkins, H., Sbrana, E., Kolli, D., Garofalo, R.P., and Rajarathnam, K. (2015). Chemokine CXCL1-Mediated Neutrophil Trafficking in the Lung: Role of CXCR2 Activation. J Innate Immun *7*, 647–658.

40. Hijano, D.R., Vu, L.D., Kauvar, L.M., Tripp, R.A., Polack, F.P., and Cormier, S.A. (2019). Role of Type I Interferon (IFN) in the Respiratory Syncytial Virus (RSV) Immune Response and Disease Severity. Front Immunol *10*.

41. Brodsky, N.N., Ramaswamy, A., and Lucas, C.L. (2020). The Mystery of MIS-C Post-SARS-CoV-2 Infection. Trends in Microbiology *28*, 956–958.

42. Esteve-Sole, A., Anton, J., Pino-Ramírez, R.M., Sanchez-Manubens, J., Fumadó, V., Fortuny, C., Rios-Barnes, M., Sanchez-de-Toledo, J., Girona-Alarcón, M., Mosquera, J.M., et al. (2021). Similarities and differences between the immunopathogenesis of COVID-19-related pediatric inflammatory multisystem syndrome and Kawasaki disease. J Clin Invest.

43. Goodnow, C.C. (2021). COVID-19, varying genetic resistance to viral disease and immune tolerance checkpoints. Immunology & Cell Biology *99*, 177–191.

44. D'Ignazio, L., and Rocha, S. (2016). Hypoxia Induced NF-κB. Cells *5*.

45. D'Ignazio, L., Bandarra, D., and Rocha, S. (2016). NF-κB and HIF crosstalk in immune responses. FEBS J *283*, 413–424.

46. Bastard, P., Rosen, L.B., Zhang, Q., Michailidis, E., Hoffmann, H.-H., Zhang, Y., Dorgham, K., Philippot, Q., Rosain, J., Béziat, V., et al. (2020). Autoantibodies against type I IFNs in patients with life-threatening COVID-19. Science *370*.

47. Hadjadj, J., Yatim, N., Barnabei, L., Corneau, A., Boussier, J., Smith, N., Péré, H., Charbit, B., Bondet, V., Chenevier-Gobeaux, C., et al. (2020). Impaired type I interferon activity and inflammatory responses in severe COVID-19 patients. Science *369*, 718–724.

48. Zhang, Q., Bastard, P., Liu, Z., Pen, J.L., Moncada-Velez, M., Chen, J., Ogishi, M., Sabli, I.K.D., Hodeib, S., Korol, C., et al. (2020). Inborn errors of type I IFN immunity in patients with life-threatening COVID-19. Science *370*.

49. Combes, A.J., Courau, T., Kuhn, N.F., Hu, K.H., Ray, A., Chen, W.S., Chew, N.W., Cleary, S.J., Kushnoor, D., Reeder, G.C., et al. (2021). Global absence and targeting of protective immune states in severe COVID-19. Nature, 1–10.

50. Sehgal, K., Guo, X., Koduru, S., Shah, A., Lin, A., Yan, X., and Dhodapkar, K.M. (2013). Plasmacytoid dendritic cells, interferon signaling, and FcγR contribute to pathogenesis and therapeutic response in childhood immune thrombocytopenia. Sci Transl Med *5*, 193ra89.

51. Amoah, B.P., Yang, H., Zhang, P., Su, Z., and Xu, H. (2015). Immunopathogenesis of Myocarditis: The Interplay Between Cardiac Fibroblast Cells, Dendritic Cells, Macrophages and CD4+T Cells. Scandinavian Journal of Immunology *82*, 1–9.

52. Calabrese, F., Carturan, E., Chimenti, C., Pieroni, M., Agostini, C., Angelini, A., Crosato, M., Valente, M., Boffa, G.M., Frustaci, A., et al. (2004). Overexpression of tumor necrosis factor (TNF) α and TNF α receptor I in human viral myocarditis: clinicopathologic correlations. Modern Pathology *17*, 1108–1118.

53. Mann Douglas L. (2001). Tumor Necrosis Factor and Viral Myocarditis: The Fine Line Between Innate and Inappropriate Immune Responses in the Heart. Circulation *103*, 626–629.

54. Angelo, L.S., and Kurzrock, R. (2007). Vascular Endothelial Growth Factor and Its Relationship to Inflammatory Mediators. Clin Cancer Res *13*, 2825–2830.

55. Delprat, V., Tellier, C., Demazy, C., Raes, M., Feron, O., and Michiels, C. (2020). Cycling hypoxia promotes a pro-inflammatory phenotype in macrophages via JNK/p65 signaling pathway. Scientific Reports *10*, 882.

56. Hua Xiumeng, Hu Gang, Hu Qingtao, Chang Yuan, Hu Yiqing, Gao Linlin, Chen Xiao, Yang Ping-Chang, Zhang Yu, Li Mingyao, et al. (2020). Single-Cell RNA Sequencing to Dissect the Immunological Network of Autoimmune Myocarditis. Circulation *142*, 384–400.

57. Maloney, J.P., and Gao, L. (2015). Proinflammatory Cytokines Increase Vascular Endothelial Growth Factor Expression in Alveolar Epithelial Cells. Mediators of Inflammation *2015*, e387842. https://www.hindawi.com/journals/mi/2015/387842/.

58. Vella, L.A., Giles, J.R., Baxter, A.E., Oldridge, D.A., Diorio, C., Kuri-Cervantes, L., Alanio, C., Pampena, M.B., Wu, J.E., Chen, Z., et al. (2021). Deep immune profiling of MIS-C demonstrates marked but transient immune activation compared to adult and pediatric COVID-19. Science Immunology *6*.

59. Qin, C., Zhou, L., Hu, Z., Zhang, S., Yang, S., Tao, Y., Xie, C., Ma, K., Shang, K., Wang, W., et al. (2020). Dysregulation of immune response in patients with COVID-19 in Wuhan, China. Clin Infect Dis.

60. Zhou, Y., Fu, B., Zheng, X., Wang, D., Zhao, C., Qi, Y., Sun, R., Tian, Z., Xu, X., and Wei, H. (2020). Pathogenic T-cells and inflammatory monocytes incite inflammatory storms in severe COVID-19 patients. Natl Sci Rev *7*, 998–1002.

61. Belhadjer, Z., Méot, M., Bajolle, F., Khraiche, D., Legendre, A., Abakka, S., Auriau, J., Grimaud, M., Oualha, M., Beghetti, M., et al. (2020). Acute Heart Failure in Multisystem Inflammatory Syndrome in Children in the Context of Global SARS-CoV-2 Pandemic. Circulation *142*, 429–436.

62. Szekely Yishay, Lichter Yael, Taieb Philippe, Banai Ariel, Hochstadt Aviram, Merdler Ilan, Gal Oz Amir, Rothschild Ehud, Baruch Guy, Peri Yogev, et al. (2020). Spectrum of Cardiac Manifestations in COVID-19. Circulation *142*, 342–353.

63. Guo, T., Fan, Y., Chen, M., Wu, X., Zhang, L., He, T., Wang, H., Wan, J., Wang, X., and Lu, Z. (2020). Cardiovascular Implications of Fatal Outcomes of Patients With Coronavirus Disease 2019 (COVID-19). JAMA Cardiol *5*, 811.

64. Lala, A., Johnson, K.W., Januzzi, J.L., Russak, A.J., Paranjpe, I., Richter, F., Zhao, S., Somani, S., Van Vleck, T., Vaid, A., et al. (2020). Prevalence and Impact of Myocardial Injury in Patients Hospitalized With COVID-19 Infection. Journal of the American College of Cardiology *76*, 533–546.

65. Lindner, D., Fitzek, A., Bräuninger, H., Aleshcheva, G., Edler, C., Meissner, K., Scherschel, K., Kirchhof, P., Escher, F., Schultheiss, H.-P., et al. (2020). Association of Cardiac Infection With SARS-CoV-2 in Confirmed COVID-19 Autopsy Cases. JAMA Cardiol *5*, 1281.

66. Metkus Thomas S., Sokoll Lori J., Barth Andreas S., Czarny Matthew J., Hays Allison G., Lowenstein Charles J., Michos Erin D., Nolley Eric P., Post Wendy S., Resar Jon R., et al. (2021). Myocardial Injury in Severe COVID-19 Compared With Non–COVID-19 Acute Respiratory Distress Syndrome. Circulation *143*, 553–565.

67. Bearse, M., Hung, Y.P., Krauson, A.J., Bonanno, L., Boyraz, B., Harris, C.K., Helland, T.L., Hilburn, C.F., Hutchison, B., Jobbagy, S., et al. (2021). Factors associated with myocardial SARS-CoV-2 infection, myocarditis, and cardiac inflammation in patients with COVID-19. Modern Pathology, 1–13.

68. Zimmermann, P., and Curtis, N. (2020). Coronavirus Infections in Children Including COVID-19: An Overview of the Epidemiology, Clinical Features, Diagnosis, Treatment and Prevention Options in Children. Pediatr Infect Dis J *39*, 355–368.

69. CDC (2020). Multisystem Inflammatory Syndrome in Children (MIS-C) Associated with Coronavirus Disease 2019 (COVID-19). https://emergency.cdc.gov/han/2020/han00432.asp.

70. Brissaud, O., Botte, A., Cambonie, G., Dauger, S., de Saint Blanquat, L., Durand, P., Gournay, V., Guillet, E., Laux, D., Leclerc, F., et al. (2016). Experts' recommendations for the management of cardiogenic shock in children. Ann Intensive Care *6*, 14.

71. Canter Charles E. and Simpson Kathleen E. (2014). Diagnosis and Treatment of Myocarditis in Children in the Current Era. Circulation *129*, 115–128.

72. Darnell, M.E.R., and Taylor, D.R. (2006). Evaluation of inactivation methods for severe acute respiratory syndrome coronavirus in noncellular blood products. Transfusion *46*, 1770–1777.

73. Rodero, M.P., Decalf, J., Bondet, V., Hunt, D., Rice, G.I., Werneke, S., McGlasson, S.L., Alyanakian, M.-A., Bader-Meunier, B., Barnerias, C., et al. (2017). Detection of interferon alpha protein reveals differential levels and cellular sources in disease. J Exp Med *214*, 1547–1555.

74. Grzelak, L., Temmam, S., Planchais, C., Demeret, C., Tondeur, L., Huon, C., Guivel-Benhassine, F., Staropoli, I., Chazal, M., Dufloo, J., et al. (2020). A comparison of four serological assays for detecting anti-SARS-CoV-2 antibodies in human serum samples from different populations. Sci Transl Med *12*.

75. Bagwell, C.B., Inokuma, M., Hunsberger, B., Herbert, D., Bray, C., Hill, B., Stelzer, G., Li, S., Kollipara, A., Ornatsky, O., et al. (2020). Automated Data Cleanup for Mass Cytometry. Cytometry A *97*, 184–198.

76. Van Gassen, S., Callebaut, B., Van Helden, M.J., Lambrecht, B.N., Demeester, P., Dhaene, T., and Saeys, Y. (2015). FlowSOM: Using self-organizing maps for visualization and interpretation of cytometry data. Cytometry A *87*, 636–645.

77. McInnes, L., Healy, J., and Melville, J. UMAP: Uniform Manifold Approximation and Projection for Dimension Reduction. 63.

78. Stuart, T., Butler, A., Hoffman, P., Hafemeister, C., Papalexi, E., Mauck, W.M., Hao, Y., Stoeckius, M., Smibert, P., and Satija, R. (2019). Comprehensive Integration of Single-Cell Data. Cell *177*, 1888-1902.e21.

79. Monaco, G., Lee, B., Xu, W., Mustafah, S., Hwang, Y.Y., Carré, C., Burdin, N., Visan, L., Ceccarelli, M., Poidinger, M., et al. (2019). RNA-Seq Signatures Normalized by mRNA Abundance Allow Absolute Deconvolution of Human Immune Cell Types. Cell Rep *26*, 1627-1640.e7.

80. Rosenberg, B.R., Freije, C.A., Imanaka, N., Chen, S.T., Eitson, J.L., Caron, R., Uhl, S.A., Zeremski, M., Talal, A., Jacobson, I.M., et al. (2018). Genetic Variation at IFNL4 Influences Extrahepatic Interferon-Stimulated Gene Expression in Chronic HCV Patients. J Infect Dis *217*, 650–655.

81. Kim, D., Paggi, J.M., Park, C., Bennett, C., and Salzberg, S.L. (2019). Graph-based genome alignment and genotyping with HISAT2 and HISAT-genotype. Nat Biotechnol *37*, 907–915.

82. Love, M.I., Huber, W., and Anders, S. (2014). Moderated estimation of fold change and dispersion for RNA-seq data with DESeq2. Genome Biol *15*, 550.

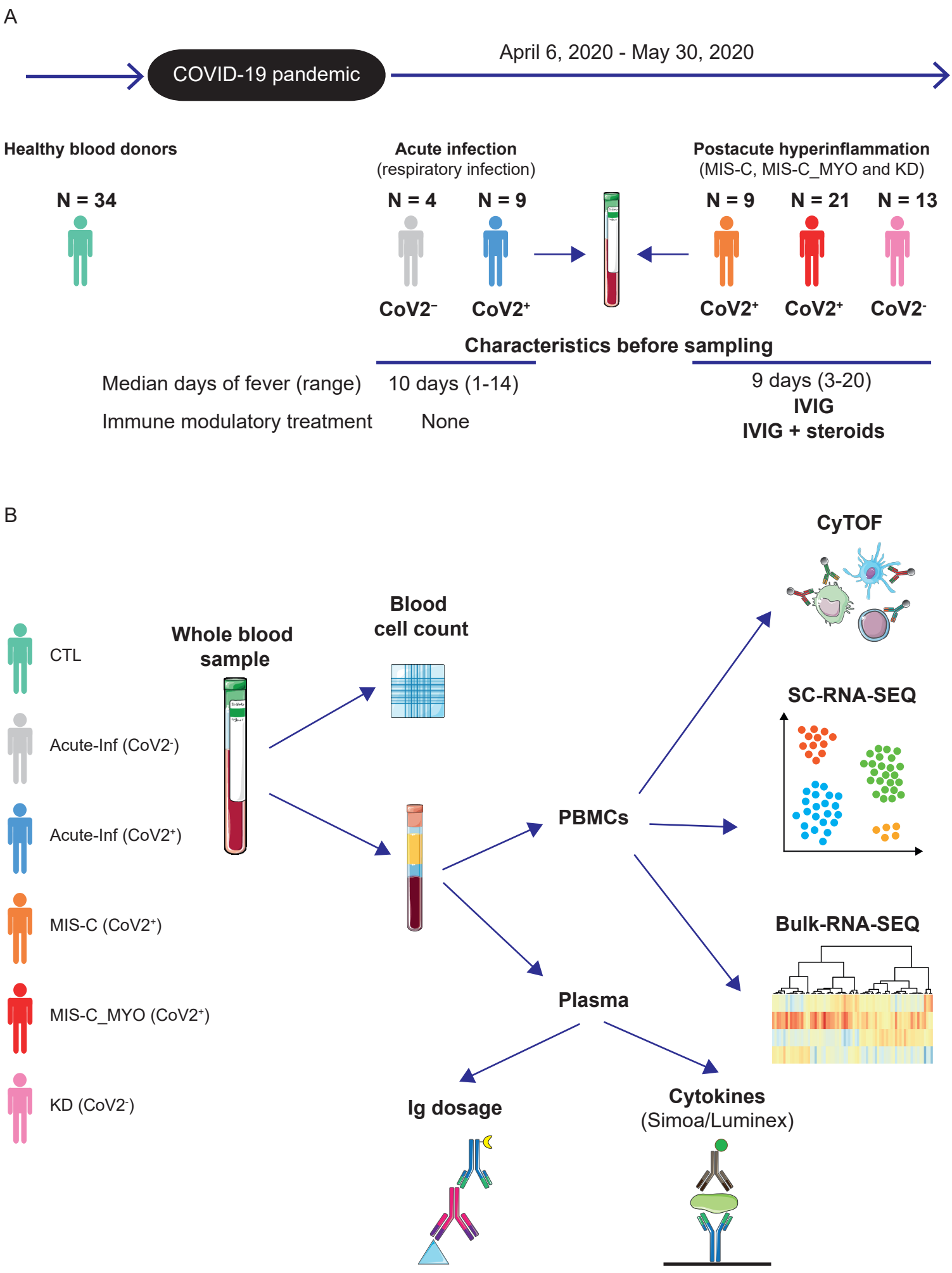

Figure 1: Timeline and experimental designs

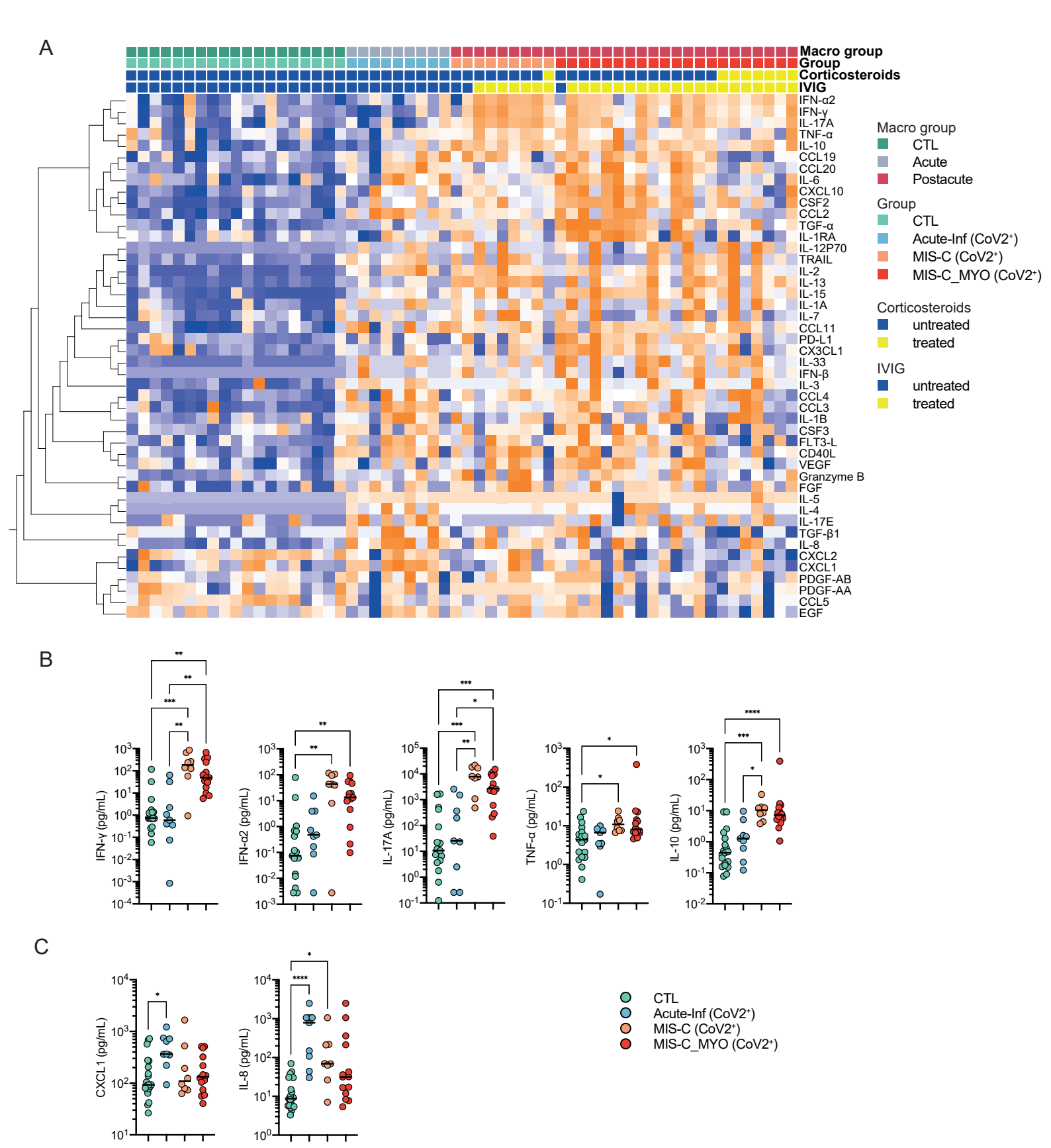

Figure 2: Analyses of cytokine/chemokine plasma levels

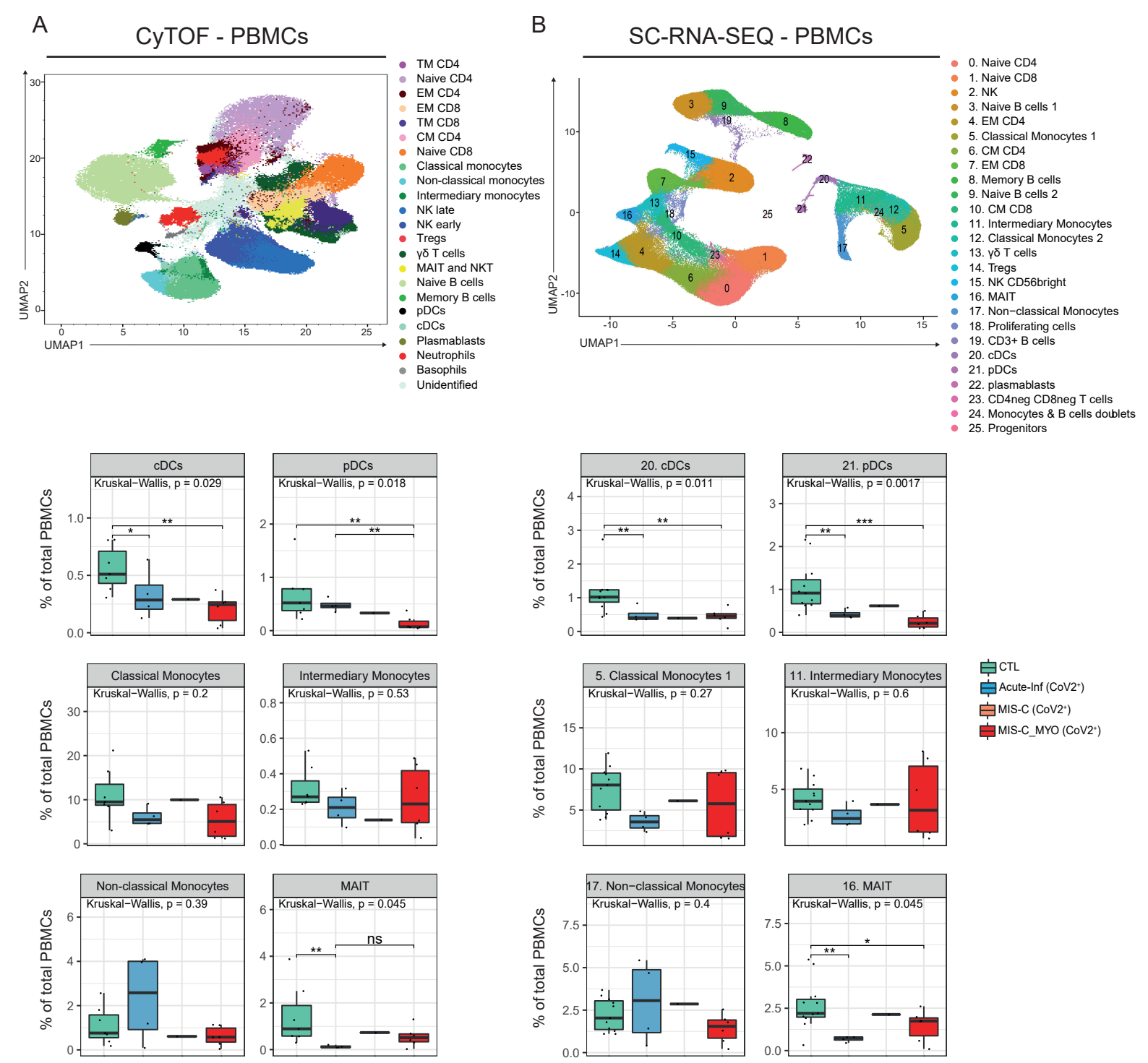

Figure 3: CyTOF and SC-RNA-SEQ characterization of PBMCs distribution

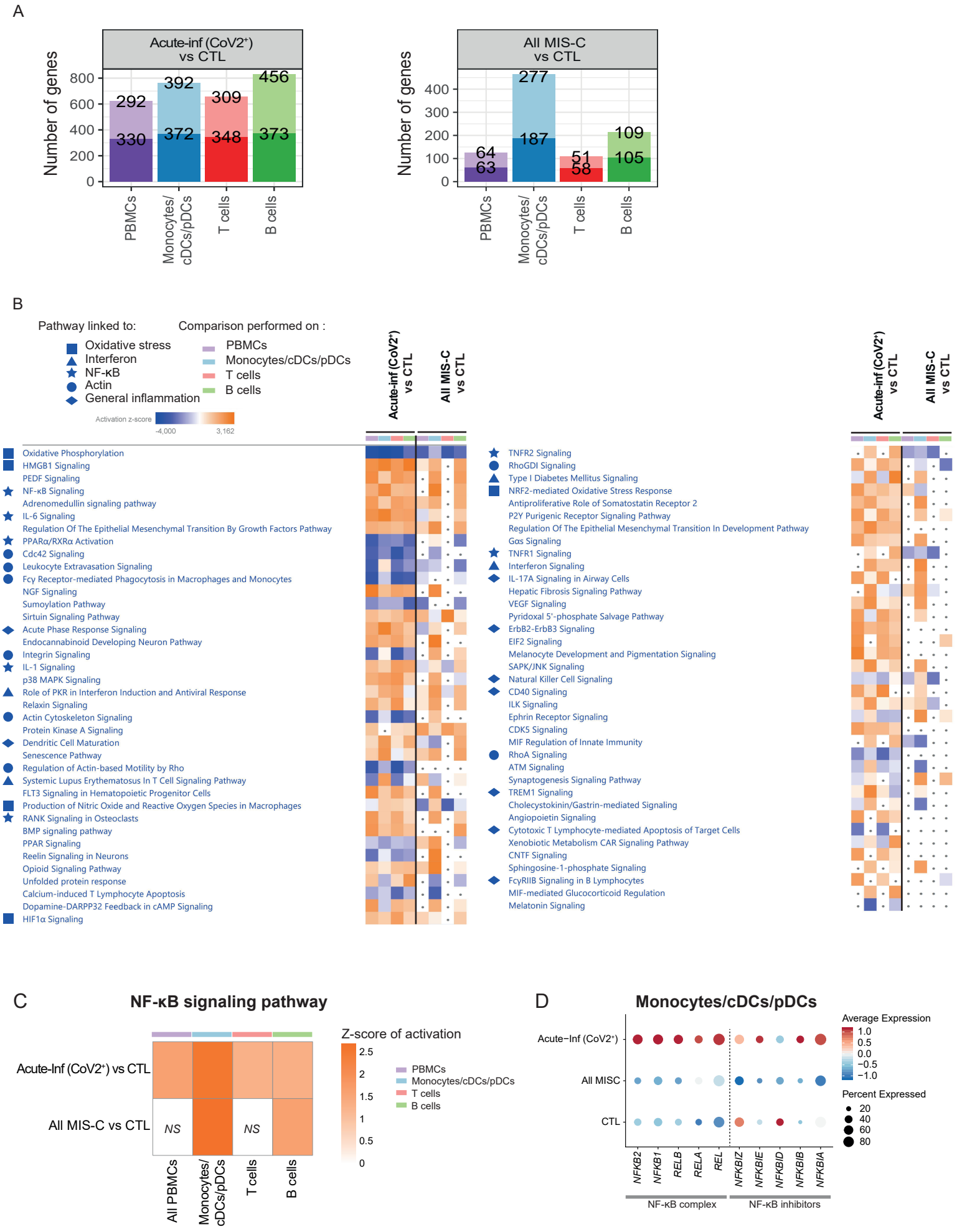

Figure 4: Genes and pathways differentially regulated in acute infection and postacute hyper inflammation following SARS-CoV-2 infection

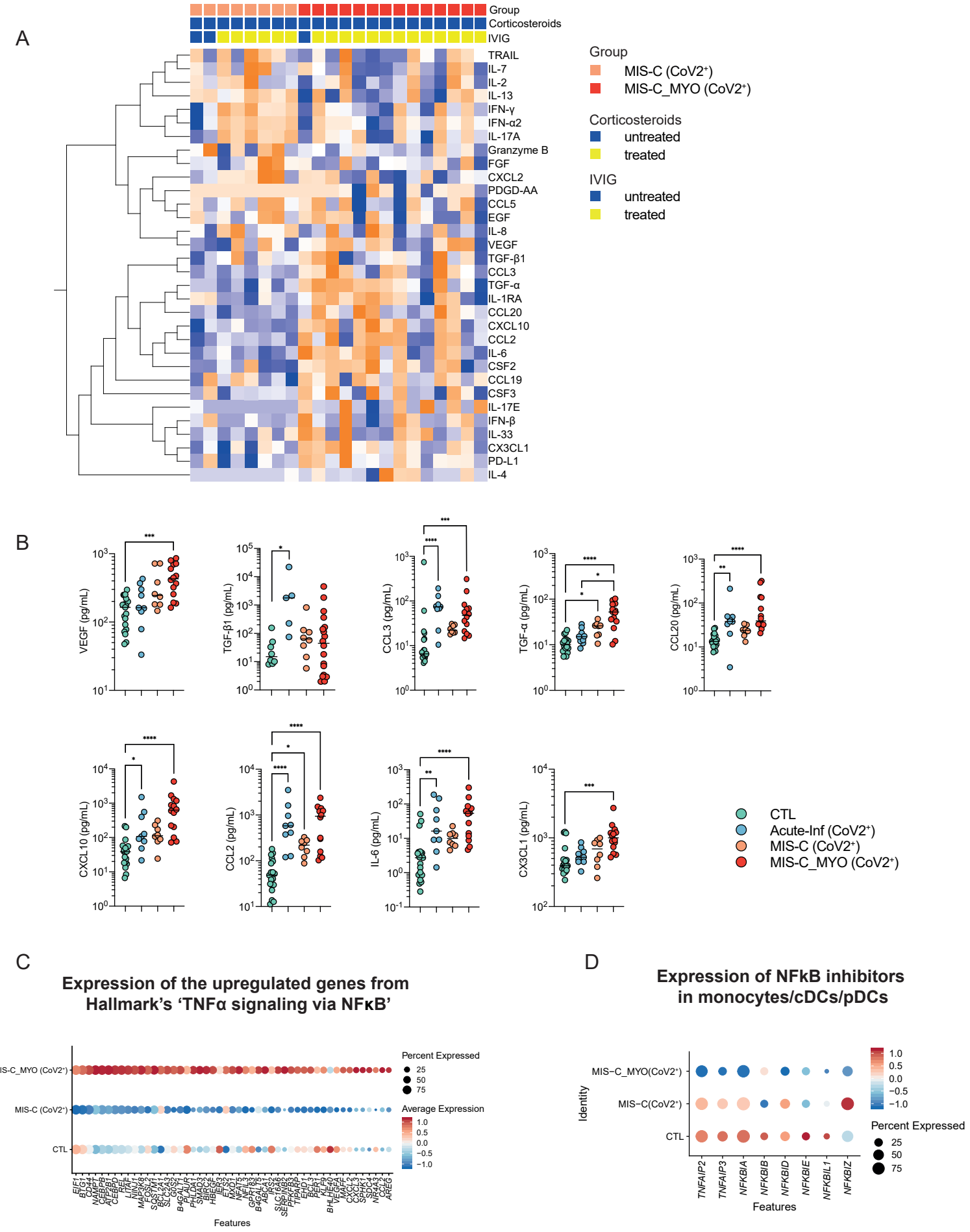

Figure 5: Cytokine/chemokine and gene expression analyses reveal an exacerbation of TNF-α and NF-κB signaling pathways in MIS-C_MYO (CoV2+) as compared to MIS-C (CoV2+)

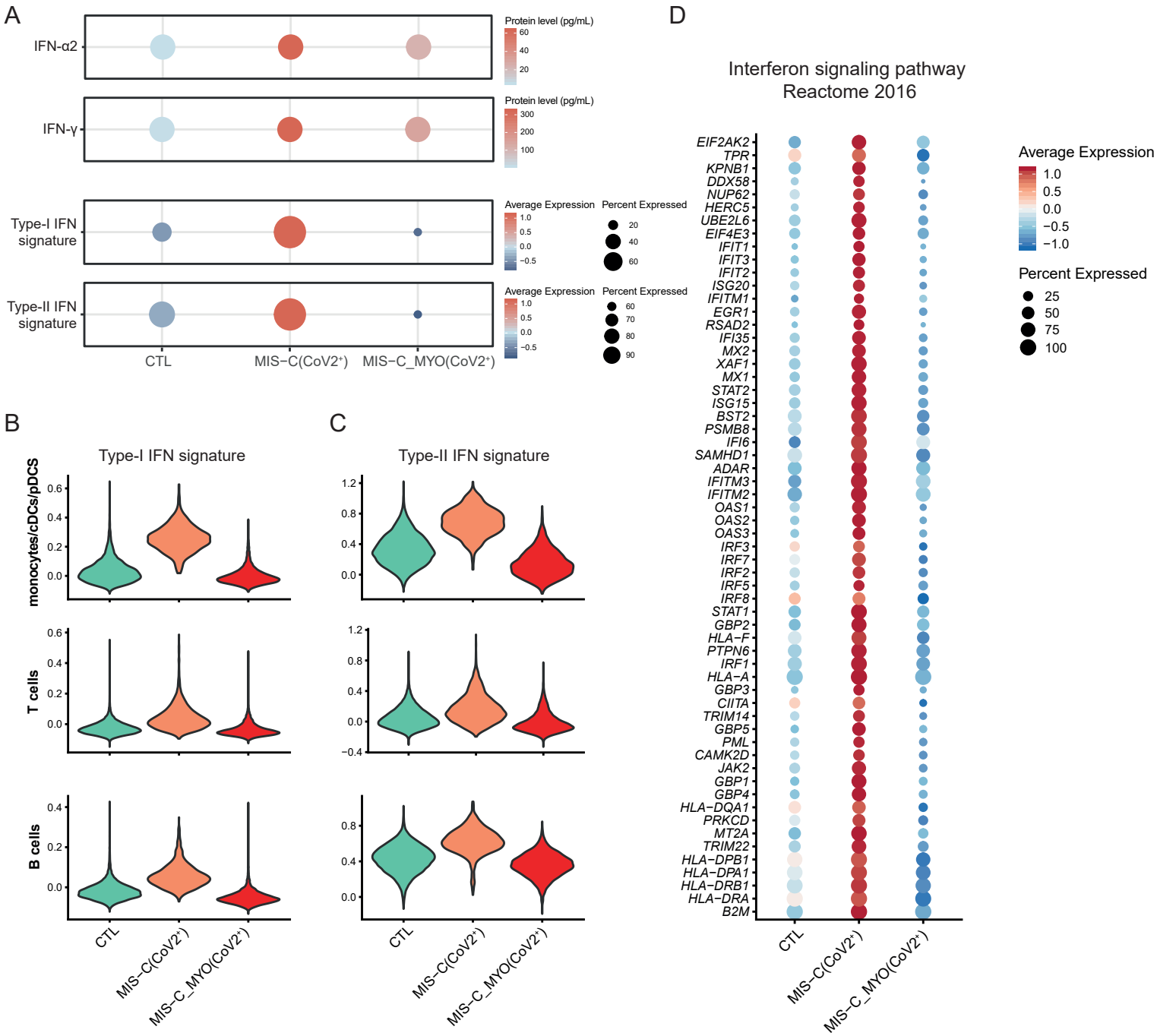

Figure 6: Differences in Interferon responses between MIS-C (CoV2⁺) and MIS-C_MYO (CoV2⁺)

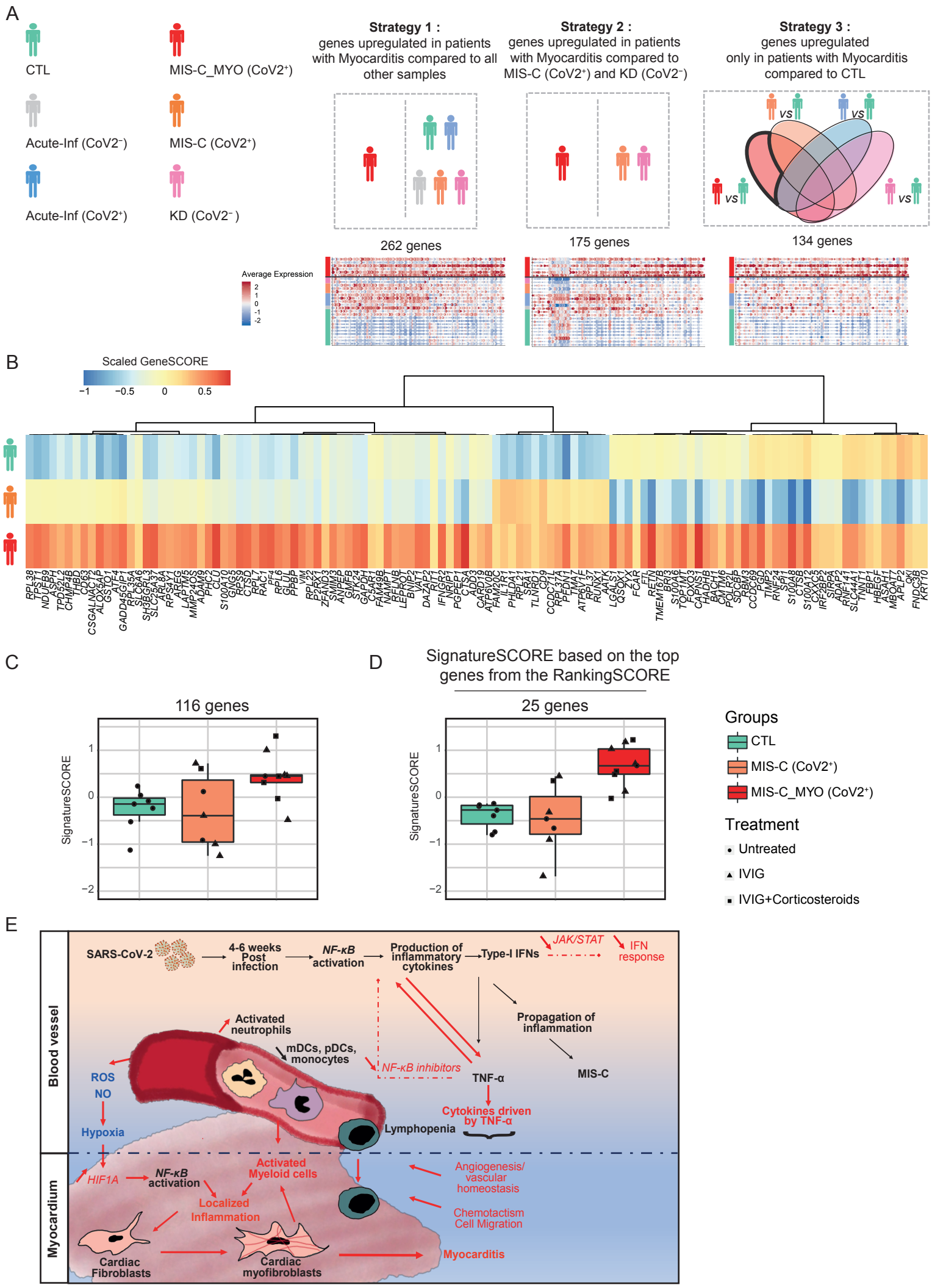

Figure 7: Molecular signature and proposed mechanism associated with severe myocarditis in children with MIS-C

SARS-CoV-2

4-6 weeks post-infection

Multisystem Inflammatory Syndrome in Children (MIS-C)

- Ig dosage
- Cytokines
- CyTOF
- SC-RNA-SEQ
- Bulk-RNA-SEQ

IFN-γ, IFN-α2, IL-17A, TNF-α, IL-10

mDCs, pDCs, monocytes

NF-κB activation

Without severe myocarditis

Type-I and Type-II IFN responses

NF-κB Inhibitors

IL-6
IL-15

VEGF
TGF-α

CCL2
CX3CL1
CXCL10
GM-CSF

Hypoxia

With severe myocarditis

TNF-α signaling via NF-κB

Inflammation

IL-6
IL-15

Angiogenesis and vascular homeostasis

VEGF
TGF-α

Chemotaxis and Cell migration

CCL2
CX3CL1
CXCL10
GM-CSF

Hypoxia

Signature to discriminate MIS-C with severe myocarditis

SC-RNA-SEQ

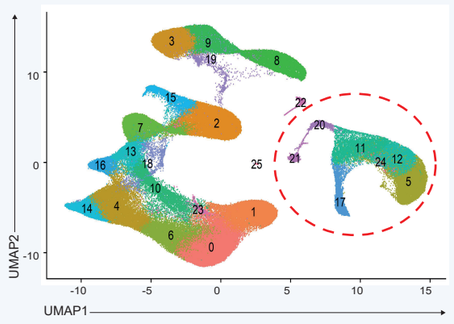

329 genes upregulated in DCs/monocytes

Bulk-RNA-SEQ

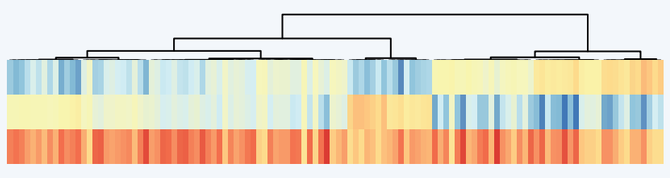

Validation of 116 genes in PBMCs

Molecular signature

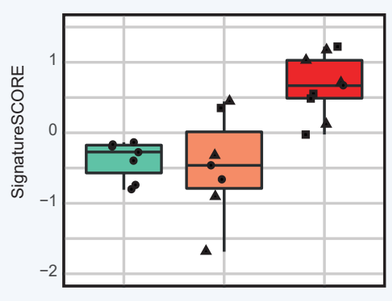

Top 25 genes